ANU-P/978
May 1988

THE IDENTIFICATION AND REJECTION OF ENERGY-DEGRADED EVENTS IN GAS IONIZATION COUNTERS

T.R. Ophel, L.K. Fifield, W.N. Catford, N.A. Orr, C.L. Woods,
A. Harding and G.P. Clarkson.

Department of Nuclear Physics, Research School of Physical Sciences,
Australian National University, GPO Box 4, Canberra, ACT 2601, Australia.

Accepted for publication in NIM.

ANU-P/978
MAY 1988

THE IDENTIFICATION AND REJECTION OF ENERGY-DEGRADED EVENTS IN GAS IONIZATION COUNTERS

T.R. OPHEL, L.K. FIFIELD, W.N. CATFORD, N.A. ORR, C.L. WOODS, A. HARDING and G.P. CLARKSON.

Department of Nuclear Physics,
Research School of Physical Sciences,
Australian National University,
G.P.O. Box 4, Canberra, A.C.T. 2601, Australia.

Abstract

A common feature of the measurement of charged particles with gas detectors is the presence of a small fraction of events (~0.1-0.2%) for which significantly less than the total ionization is recorded. These events cause an energy tailing that can seriously impair the identification functions of gas detectors used either to instrument the focal plane of magnetic spectrometers or for accelerator mass spectrometry.

The anomalous, energy-degraded events are shown to arise both from reactions between the incident ions and the detector gas and, more importantly, from the scattering of ions by the gas. It is demonstrated that an appropriate detector configuration provides the means to reject most of the anomalous events, allowing the measurement of very low cross-section reactions without significant background interference from such events.

1. Introduction

Gas-filled, multi-electrode detectors have become the standard instrumentation for the focal planes of magnetic spectrometers[1]. Typically, measurements of the total incident energy (E_T), one or more energy losses (ΔE_1, ΔE_2 etc) and two position signals (P_1 & P_2) to determine distance along the focal plane and the angle of entry, provide excellent identification of ion mass (m), atomic number (Z) and atomic charge state (q).

As well as proving to be extremely versatile for general reaction studies, such detectors have demonstrated their outstanding characteristics in the clean separation of the products of extremely low cross-section reactions from products of competing reactions many orders of magnitude more intense. Background-free spectra of many neutron-rich or "exotic" nuclei have been obtained for which accurate mass measurements and structure information have been deduced[2].

Simpler detectors, measuring only E_T, ΔE and the residual energy (E_R) deposited near the end of the stopping length in the gas, have been used for accelerator mass spectrometry (A.M.S.). Again, excellent separation, between for example ^{36}S and ^{36}Cl or ^{41}K and ^{41}Ca, is usually straightforward.

However difficulties have been encountered in both types of application due to the presence of energy-degraded events. These events are evident as tailing of both the E_T and E_R signals, extending down beyond 50% of the correct value. For example, an attempt to measure the mass of ^{20}N, using the reaction $^{48}Ca(^{18}O,^{20}N)^{46}Sc$, was frustrated by such background tailing[3]. Although ^{20}N ions were clearly observed, (figure 1), energy-degraded events from relatively intense $^{17}O^{7+}$ ions prevented unambiguous identification of the ground state group in a projected P_1 spectrum. For

the same magnetic rigidity, $^{17}O^{7+}$ and $^{20}N^{7+}$ ions have energies differing by ~18% so that their initial rates of energy loss (as measured by ΔE_1) are almost identical. Separation is therefore reliant on a correct energy measurement. In the case of accelerator mass spectrometry, Tuniz et al[4] reported backgrounds from intense ^{9}Be ions interfering with the identification of ^{10}Be ions because "some (^{9}Be ions) however evidently fail to deposit all their energy".

The present investigation sought to identify the origin of the energy tailing and to develop the means of overcoming the problems caused by it.

2. Anomalous events observed with focal plane detectors

Typically, a variety of low level ($\lesssim$ 1%) backgrounds[a] is observed with gas-filled, focal plane detectors. A schematic representation of the common anomalous or background effects is shown in Figure 2 which depicts a situation where three charge states of a single, intense ion species (from elastic scattering, for example) are deflected into a detector. Four types of events occur for which either or both the total energy and the position signals differ from the values associated with the majority of the ion events. These are identified as:-

2.1 Slit or edge scattering which is a component having the same E_T and P characteristics as lower energy ions of the same species. These arise mainly from edge scattering at defining collimators before the target and at apertures between the target and the magnetic spectrometer. Since these

---

a Backgrounds of external origin, such as from neutrons and cosmic rays, are not considered. Only effects due to clearly identified charged particles entering a detector are relevant.

events have the correct m/q^2 (i.e. P_1^2/E) and $E.\Delta E$ values, they comprise a background tail in the position distribution, obscuring weak inelastic events and reaction products at very forward angles.

Often the intensity of such events can be significantly reduced by constraints on the angle of entry of ions into the detector[5] or by carrying out measurements without beam collimation[6].

2.2 Charge exchange in flight between the target and the detector. These events have the same total energy as the primary ion species but have a continuous distribution of deflection (P_1) along the focal plane. Even in extreme cases where the spectrometer vacuum is poor (>10^{-5} torr), the fact that events due to such ions have very different angles of entry into the detector allows them to be readily identified and rejected.

The effect can be exploited for studies of electron conversion lifetimes[7].

2.3 Pulse pile-up due to ions arriving almost simultaneously at the detector. For a single group,[b] position derivation is unaffected but the detected energy (and $\Delta E, E_R$) extends to twice that associated with a single ion. Pile-up events mainly constitute a background for isotopes with different q, e.g. pulse pile-up from $^{18}O^{7+}$ ions interferes with $^{22}O^{8+}$ identification.

In some cases, the effect may be suppressed by pulse height or transit time constraints on the signals from either the resistive wire or delay line

---

b More generally, when two ions arrive simultaneously at different distances along the detector, the derived position will fall between the individual positions.

used to determine the position. However, standard electronic pile-up rejection techniques are more generally applicable and have successfully overcome the problem[8].

2.4 Energy-degraded events manifested as a tailing of the energy distribution for monoenergetic ions arriving and being detected at the same position on the focal plane.

The fraction of events in the tail, measured at various laboratories with detectors of widely varying dimensions for a variety of ion types and energies (e.g. 34 MeV ^{7}Li to 400 MeV ^{48}Ti), ranges from about 0.06% to 0.2%[9]. For any particular detector, the fraction is essentially independent of ion type and energy.[c] The present investigation was directed toward the origin and identification of these events.

3. Mechanisms for the production of energy-degraded events

In view of the low pressures at which the detectors normally operate and the fact that the fraction of the tail events is not a strong function of ion species, ion recombination near the end of the ion path is not likely to be significant. However, there are a number of other processes which occur in the gas of the detector and would cause energy-degraded events.

a) Reactions with the stopping gas

Fusion reactions between the incident primary ions and constituent

---

c Tailing (~1%) can occur when the vertical height of the image of a deflected group exceeds that of the entrance aperture. Edge penetration of the window support can then cause extreme tailing. Such an effect is not included in the present discussion.

nuclei of the stopping gas (usually isobutane) would result in the subsequent emission of neutrons, protons, α-particles and gamma rays which carry an appreciable amount of the initial energy but deposit little or none of it in the detector.

b) Scattering of the incident ions

Some ions will undergo elastic and inelastic scattering from the carbon and hydrogen constituents of isobutane (C_4H_{10}). For purely Rutherford scattering, the predominant contribution over most of the ion path length would be from the hydrogen since the effects of the much lower centre of mass energy and greater number of hydrogen atoms outweigh the Z-dependence. For ^{16}O ions of a given energy, the hydrogen scattering cross-section is a factor of 22.1 larger than that for carbon. The recoiling protons and carbon ions will generally have energy loss rates lower than those of the primary ions. In fact, scattering by protons would result in essentially the complete loss of the recoil energy whereas some or all of the recoil energy of carbon ions would be expended in the gas of the detector. In the extreme case of head-on elastic collisions, proton recoils acquire 22%, and carbon recoils 98%, of the energy of primary ^{16}O ions. Thus it is reasonable to suppose that the higher energy degraded events are mainly the result of hydrogen scattering and that events below ~ 80% of the incident primary ion (^{16}O) energy are due to scattering by carbon. A small fraction of the ions will undergo relatively large angle scattering from the carbon in the isobutane and either the scattered primary ion or the recoiling ion may strike the cathode electrode or wires of the grid, thereby reducing the total energy lost in the gas. In double-gridded detectors, similar scattering through the first grid (defining the volume in which E_T is measured) is more complex. The magnitudes of both the E_T and anode

signals would be little affected if ionization were produced in the region between the two grids. However, if the scattered ions penetrate beyond the second grid, both E_T and the anode signals would be reduced.

Evidence of the contributions from the various processes was accumulated from measurements with several detectors.

3.1 Reactions with the stopping gas

Investigations using a focal plane detector that has been described previously[10] (and is similar schematically to the detector in Figure 5), demonstrated that about half the energy-degraded events were distinguished by the absence of a P_2 signal and mainly with detected energies of less than 50% of the primary ions. Moreover, these events were associated with inconsistent values of ΔE_1 and ΔE_2, both of which varied from between ~10% and 200% of the values for properly detected ions.

Such events are attributed to the occurrence of fusion reactions. When isobutane is used, reactions will occur mainly in the front portion of the detector where the available centre of mass energy is highest. Obviously, rejection of the events is obtained merely by the requirement of a P_2 signal for a valid event.

3.2 Scattering by the gas.

Most of the higher energy portion of the tail was comprised of events with normal ΔE_1, ΔE_2, P_1 and P_2 signals. As would be expected, a measurement of residual energy, from the rear section of the anode plane of the detector, exhibited tailing which was correlated with that of the E_T signal.

Indirect evidence that energy degradation arises from scattering effects was obtained by reducing the detector gas pressure sufficiently to

allow the primary ion species to just reach the back wall of the detector. Under this condition, the detected energy signal was ~ 95% of the optimum signal observed at higher gas pressures but, importantly, derivation of a pulse signal from a third resistive wire at the rear of the detector (usually performing the function of vetoing events not stopped) became possible. For a narrow ray of elastically-scattered ions (0.1° spectrometer acceptance), the energy tail contained 66 events when there were 100,000 events in the peak. All of these events were associated with normal P_1, ΔE_1, ΔE_2 and P_2 signals. Imposition of the additional requirement of a P_3 signal, i.e. selection of events with the correct range, reduced the integrated peak count by <1% but removed all of the tail events.

More direct evidence was provided by several features apparent in measurements with a small, gas-filled detector used for accelerator mass spectrometry[11]. A portion of the anode of the detector, immediately preceding the final electrode used to measure residual energy, has a saw-tooth configuration[12]. When the detector is mounted with the electrodes vertical, the difference between the energy losses observed for the halves of the saw-tooth provides a simple means of determining the vertical position of each incident ion. The resolution achieved is ~1 mm.

In a typical ^{36}Cl measurement (Figure 3), many of the events exhibiting energy degradation in both E_T and E_R were associated with signals from both halves of the electrode which were larger than for normal events, i.e. an angular deflection had occurred. A comparison of the pulse heights observed on one half of the sawtooth electrode is shown in Figure 4. Rejection of 50% of the total events on the basis of the magnitude of either sawtooth signal eliminated more than 80% of the tail events of the ^{36}S peak. Further, it is evident in Figure 3 that both of the intense ^{36}S and ^{37}Cl groups are associated with a small number of events for which the E_R signal

is reduced but the correct E_T is measured. These events can be interpreted as being due to scattering events occurring before the E_R electrode for which the recoil ion (presumably ^{12}C) energies were low enough for them to be stopped in the gas and the primary ions, with a reduced energy, lost more energy before reaching the E_R electrode.

4. Aspects of detector design required for detection of energy-degraded events

The problem of energy tailing due to nuclear reactions, including elastic and inelastic scattering, occurring in detectors is a general one. Such effects have been reported for charged particles in scintillators[13] and silicon surface barrier detectors[14] and have been exploited for measurements of reactions induced by gamma rays[15] and neutrons[16]. However, multi-electrode gas detectors would appear capable of eliminating such effects since they are, in principle, able to measure the ionization produced along the entire path of each ion.

It is useful to consider the merits of the various means by which the scattered ions might be detected. In some cases, e.g the problem of discriminating between ^{20}N ions and energy-degraded ^{17}O events, the ambiguity can be resolved at the cost of added complexity by measuring the time of flight of ions between the target and the entrance to the focal plane detector. Such techniques have been described elsewhere[17].

4.1 Use of a range measurement

A range measurement is possible using either a simple anode element or a position sensing element (P_3) to detect the ionization produced at the end of the ion path. The latter overcomes the energy straggling effects, which would be evident with a simple electrode, achieving better spatial

resolution at the cost of losing straightforward, ancillary information as to the ion type being detected.

However, the demonstration in Section 3.2, that imposition of a range constraint effectively removes energy-degraded events for a single, monoenergetic group, cannot be applied generally to focal plane detectors. With detectors for which the angle of entry of detected ions is 45°, difficulties are already apparent when the simplest case of only a single, monoenergetic ion species is considered. For useful acceptance solid angles with a relatively low dispersion spectrometer, the angular spread at the focal plane will be large (typically 13.5° for an Enge split-pole spectrometer with a horizontal angular acceptance of 4.5°). Hence observation of a P_3 signal for all ions is only possible at gas pressures much lower than the pressure needed to stop them all, preventing measurement of a meaningful E_T.

With a normal entry, this difficulty is overcome. For a given ion type, there will be a small range of magnetic rigidity over which both a P_3 signal and reasonable energy (E_T) resolution can be obtained at a suitable gas pressure. However for the case of $^{17}O^{7+}$ and $^{20}N^{7+}$ mentioned previously, separation of the ion types with a detector operating at the appropriate pressure to stop the ^{20}N ions is likely to be very marginal. This situation arises because of the much greater intensity of the ^{17}O ions and the significant reduction of the difference between the measured E_T values (the ^{17}O ions would not be stopped). Furthermore, recoil ^{12}C ions could be detected by the P_3 sensor, leading to acceptance of some energy-degraded events. Additional information, such as the measurement of the residual energy beyond a P_3 element, could resolve both difficulties. However, the critical dependence of the range technique on the detector gas pressure remains a serious limitation.

4.2 Multiple energy loss measurements near the end of the range

It is evident that a detector must determine the approximate range of each ion, coupled with energy loss information along the entire ion path, to ensure that the measured signals are consistent only with the behaviour of primary ions slowing down in the gas.

Using ^{17}O and ^{20}N ions as examples once more, calculations for a variety of anode configurations suggest that effective unambiguous identification can be achieved with only two additional sensing electrodes at the end of the range. One of these would be a relatively narrow E_R electrode to define a minimum path length. The other (ΔE_{max}) immediately preceding E_R, would span the region for which dE/dx of ^{20}N ions is a maximum (i.e. the peak of the Bragg curve) when the gas pressure is set to allow the ^{20}N ions to reach E_R. Most ^{17}O ions beyond the range of magnetic rigidity of interest reach the P_3 region and thus can be vetoed. The likelihood that energy-degraded ^{17}O ions reaching E_R simultaneously produce E_T, ΔE_{max} and E_R signals which are indistinguishable from those of ^{20}N ions should be extremely small. With an E_R electrode of reasonable size (~18% of the total range), an acceptable dynamic range of ^{20}N energies is possible (~5 MeV) while maintaining a difference of ~12% between the ΔE_{max} values for ^{20}N and ^{17}O ions (^{20}N greater).

4.3 Reduction or detection of large angle scattering events

Several techniques could either reduce the number of energy-degraded events due to large angle scattering events or else provide the means to identify such events. These include:

(a) Increase of grid/cathode spacing

It would be anticipated that an increase of the grid/cathode spacing would reduce the number of energy-degraded events due to large angle scattering because the recoil ions and the scattered primary ions are more likely to be stopped in the gas. This was borne out by the performance of a small detector in which the separation between the central ion path and the cathode was 50% larger than for the detector used in Section 3. The fraction of tail events was only 0.04%[18]. A large grid/cathode spacing requires special measures to prevent field distortion at the electrode boundaries and consequent worsening of the E_T resolution. The usual technique of using a graded grid at the entrance of the detector is likely to introduce additional background problems.

(b) Measurement of vertical height of ion paths

By decoupling the grid and cathode, the vertical height of ions can be determined from the drift time between appearance of the cathode signal and the arrival of an anode pulse. Resolution of 1mm has been achieved in gas counters[12] though 2mm is more typical for focal plane detectors using isobutane[19]. Usually, it is only an average height of the ion path that is measured. For present requirements, the cathode would have to be segmented to determine separately the vertical height in various sections of the detector.

Though, in principle, deviations from the incident direction could be detected with such measurements, in combination with P_1, P_2 and P_3 information, the results given in Section 3.2 suggest that this method has only limited application.

(c) Use of a gridded cathode

If the cathode were gridded, then ions scattered through it could be detected with an additional electrode, at ground or slightly positive potential, located beneath the cathode. Most ions and associated recoils scattered close to the plane parallel to the electrodes will deposit their full energy in the gas. Thus it should be possible to detect about 50% of the large-angle scattered events that result in reduction of the E_T measurement with a sub-cathode.

5. A normal-entry detector

A small focal plane detector was constructed to evaluate several of the features discussed in Section 4.

The detector (Figure 5) closely followed the design of an earlier one[10]) except that most electrodes were constructed from printed circuit board to allow the electrode dimensions to be changed readily. The aluminium box (50cm x 20cm x 20cm) housing the electrode structure and the associated preamplifiers was mounted near the focal plane of a split-pole spectrometer, at 45° to the usual position to allow normal entry of the detected ions. The active length of the detector is ~ 12 cm. A grid, comprised of gold-plated tungsten wire, 125μm in diameter with a spacing of 2 mm and normal to the incident ion direction, was used as the cathode. Provision was made to mount sub-cathode electrodes 1cm beneath it.

5.1 Operating characteristics

Using 70 MeV ^{16}O ions scattered from a thin gold target, the resolution achieved for the total energy was 0.7% for a horizontal angular acceptance of 0.1°, increasing to only 0.86% with an angular acceptance of 4.5°. Corresponding results for the summed ($\Delta E_1 + \Delta E_2$) signal were 4.0% and 4.25%, and for E_R, 4.2% and 4.3%.

With the 0.1° acceptance, the resolutions obtained directly from the P_1, P_2 and P_3 spectra were 0.8 mm, 1.0 mm and 1.5 mm respectively.

5.2 Tail rejection using P_3

Tests using ^{18}O beams with energies of 60 and 70 MeV, scattered from gold at 10°, confirmed the earlier result that energy-degraded events did not produce a P_3 signal when the gas pressure allowed primary ions to just reach P_3. For example at 60 MeV with 1° horizontal acceptance, 99652 events with correct E_T, P_1, ΔE and P_2 values were associated with 85 energy-degraded events. Imposition of the P_3 requirement reduced the total to 99042 with only one energy-degraded event (at $0.80E_T$) remaining. At 70 MeV with 4.5° acceptance, 244 energy-degraded tail events were evident for a peak count of 192395, whereas again only one of them had a P_3 signal. The peak count was reduced to 192041. Thus at least 99% of the energy-degraded events can be eliminated with a loss of detection efficiency of considerably less than 1%.

The variation of the measured pulse heights of E_T and E_R with gas pressure is shown in Figure 6, along with the P_3 efficiencies for the ^{18}O groups scattered from gold and carbon at 60 MeV. At 126 torr, both P_3 efficiencies were >96% and the E_T pulse height of the higher energy group was 91.7% of the maximum measured at 140 torr, with a worsening of resolution by a factor of about two. Since the energies of the groups differ by 2.27 MeV, it is evident that a dynamic range of at least 3.75% of the incident energy can be used in this mode of operation.

Similar results were obtained at 70 MeV, for which the stopping pressure is 170 torr. At 150 and 160 torr, the P_3 efficiencies were >98% and E_T resolutions were 2% and 1% respectively.

A convincing demonstration that energy-degraded events result from

scattering emerged during these measurements (Figure 7). At a pressure of 150 torr, it is clear that energy-degraded tail events are related to those for which the residual energy is larger than for most events, i.e. those for which a scattering has not led to energy degradation but caused the primary ion to stop beneath the residual energy electrode rather than penetrate just beyond it. Ions yielding the larger E_R values must either undergo small angle scattering by hydrogen or carbon or scatter near the end of the range, again mainly from carbon, so that the recoil has a low enough energy to be stopped within the grid/cathode region. The measured ion directions (Figure 8) as deduced from (P_2-P_1), imply that the latter predominates since the events group about the mean direction. On the other hand, the energy-degraded events are more randomly scattered within the angle range, indicating that some of them arise from small angle scattering prior to P_2. A significant change (~10%) of the energy of an ^{16}O ion by carbon scattering requires a deflection well beyond the P_1 and P_2 limits of the elastic group used to provide the data of Figures 7 and 8. The maximum deflection of ^{16}O ions by proton scattering is only 3.5°. Thus a significant fraction of energy-degraded events is due to scattering by hydrogen in the front section of the detector.

Agreement between the measurements of E_T and E_R and those calculated with the code EFPD[5]) is sufficiently close (Figure 6) to allow prediction for experimental situations. In the case used previously as an example, viz separation of ^{17}O and ^{20}N at energies near 100 MeV, a difference in the E_T signals of ~ 4.5% (^{20}N greater) would occur between the ion species at the appropriate gas pressure (for stopping ^{20}N ions under P_3) and the corresponding difference in E_R would be ~ 8.5%. Both are only about a factor of two greater than the resolutions observed for equivalent conditions, so that separation of ^{20}N ions $\sim$ ^{17}O ions would be possible

only if intensities were comparable. Thus as anticipated in Sect 4.1 for the measurement of reference[3]), the means would have to be provided, for instance by including another anode electrode beyond P_3, to identify the majority of ^{17}O ions (~ 99.9%) which would provide a proper signal on the electrode.

5.3 The gridded cathode

Two configurations of a simple electrode below the gridded cathode were evaluated. One sensing sub-cathode electrode had the same area as the cathode while for the other, the area was restricted to that of the back half of the cathode below the E_R electrode.

Tests with a 4.5 MeV α-source indicated that both electrodes detected scattered particles with high efficiency, i.e. ~1 event per 1000 α-particles for the larger electrode. However, the gas pressure required to allow the α-particles to reach the P_3 element was too low to allow stable operation of the position wires.

When 70 MeV ^{16}O ions were used, only very small pulses, of opposite polarity from those that would have been produced by scattered ions, were observed. The magnitude of the pulses was proportional to the energy lost above the sub-cathode electrode and a pulse was observed for each incident ion, consistent with them being due to incomplete shielding by the gridded cathode.

To overcome this problem, the smaller sub-cathode electrode was replaced with a proportional detector of the same area, assembled as a grid of gold-plated tungsten wires, 25μm in diameter, with a spacing of 2 mm. When operated at voltages (2200-2400) at which cosmic rays were readily detected, some energy degraded events (~10%) were associated with a pulse from the proportional detector. Since the tests described in Section 5.2

demonstrated that many of the energy degraded events arise from hydrogen scattering at the front of the detector, the small number observed is not unexpected, but does confirm the occurrence of large angle scattering from carbon.

6. Multiple energy loss measurements

Both the normal entry focal plane detector and the gas detector designed for AMS measurements (Section 3.2) were used to evaluate several electrode configurations. The latter detector proved especially useful since it allowed simultaneous measurement of five energy losses along the path of each ion in addition to the total ionization.

6.1 Measurements with the AMS detector

Data were obtained for two ions species, 66 MeV ^{18}O and 132 MeV ^{36}S. The anode configuration is shown, along with a schematic representation of the results for ^{18}O, in Figure 9. At the isobutane gas pressure used, viz 150 torr, the ^{18}O ions stopped beyond E_R, depositing about 10% of the incident energy under the final anode electrode from which no signal was derived. The actual data (selected with appropriate ΔE_1 and ΔE_2 limits) for the ΔE_{max} signal as a function of E_T are shown in Figure 10. The origins of the various anomalous events are indicated on the basis of the discussion that follows. In addition, events with ΔE_3 values outside of the normal limits and those without an associated E_R signal are identified since the information provides the basis for the proposed origins.

The response of each electrode can be used to identify anomalous events occurring before, under and beyond it. Clearly anomalous events occurring beyond any particular electrode should provide a normal signal from that electrode whereas events before or under the electrode generally

will not. Several features are immediately apparent from Figure 9, viz that most of the anomalous events contributing to the energy-degraded tail occur under ΔE_3 and ΔE_{max} and that, as would be expected, the lower energy limit of the tail increases with the number of electrode signal constraints. Further, the ΔE_3, ΔE_{max} and E_R distributions reveal a successively increasing number of events with larger than normal signals, but associated with the correct total energy. No similar events are evident in the ΔE_2 (and ΔE_1) distributions. Such effects are consistent with the fact that, after a scattering, complete capture of the initial ion energy becomes increasingly probable as the ion energy (and therefore the recoil energy) decreases. The correct total energy is obtained from almost all scattering events under E_R since there are few energy-degraded events with a correct ΔE_{max} value evident in Figure 10.

Inspection of each successive pair of electrode signals, i.e. ΔE_2 and ΔE_3, ΔE_3 and ΔE_{max}, and ΔE_{max} and E_R, allows a more straightforward appraisal of the measurements (Figure 11). Few scatterings occur under ΔE_1 and ΔE_2 and most are associated with ΔE_3 signals not very different from the correct value. Thus reactions, as distinct from scattering, play a minor role at the relatively low ^{18}O energy used, although some extreme values of ΔE_2 and ΔE_3 do occur outside of the range shown in Figure 11. The greatest number of scatterings per unit electrode length obtain for the ΔE_{max} and E_R electrodes, consistent with the energy dependence of Rutherford scattering. Many yield the correct E_T value, indicating that they result from carbon scattering because the larger values of ΔE_{max} associated with them imply scatterings in which the ^{18}O energy is reduced by as much as 4 MeV. The remaining length of the detector corresponds to the range of only ~ 1.5 MeV protons but is sufficient to stop ~ 20 MeV ^{12}C ions.

More important are the energy-degraded events, with larger than normal ΔE_{max} values, because they generally affect the ability to discriminate between ion species. In Figure 10, most are close to either the locus applicable to lower energy ^{18}O ions entering the detector or to the locus calculated for scatterings under ΔE_{max} for which none of the recoil energy is deposited in the gas. Most of the former can be rejected by imposition of appropriate ΔE_3 limits (with some leakage due to finite resolution). Both types of events must be due almost entirely to scattering by hydrogen. The extent of the energy-degraded events in Window II of Figure 10 (an approximately comparable situation to $^{17}O/^{20}N$ separation discussed in Section 4.2) is sensitive to the limits chosen for ΔE_3; increasing from $0.88E_T$ with no ΔE_3 limits to $0.91\ E_T$ when a limit including all normal events is used, and to $0.93E_T$ with reduced limits rejecting 10% of the normal events.

Finally, there is a weak class of events, originating under the ΔE_{max} electrode that is characterized by a lower than normal ΔE_{max} signal. These events extend from the correct E_T value to a measured energy almost 20 MeV lower. The energy of the ^{18}O ions arriving under ΔE_{max} is ~20 MeV so that many of the events can only arise from carbon scattering or, less likely, reactions with hydrogen.[d] It is plausible to attribute such events to large angle scattering from carbon. At extreme angles (the maximum scattering angle for ^{18}O ions is 41.8°), ions scattered in the vertical

---

d Interestingly, the ^{18}O energy under the ΔE_{max} electrode traverses a strong (p,α) resonance at 15.19 MeV (equivalent to a proton energy of 844 keV). The reaction is exothermic (Q=3.98 MeV), so that for reaction events in which the recoil ^{15}N is emitted close to 0°, more than the primary energy should be measured. No such events are evident in Figure 10.

plane can strike the cathode or penetrate the grid so that, consistent with the measurements, no E_R signal will eventuate (the channel number corresponding to the minimum energy deposited by ^{18}O ions reaching E_R is ~780 in Figure 10). At more forward angles, ΔE_{max} would be reduced since the maximum increase of ΔE_{max} for a reduced ^{18}O energy is only about 10% (Figure 10), whereas the energy loss of the companion ^{12}C recoil under ΔE_{max} is some 30% less. For most of such scatterings, either or both scattered particles reach the side walls of the detector or scatter into the electrodes before expending their full energy.

The energy-degraded events stemming from carbon scattering demonstrate the value of an intermediate electrode preceding the E_R electrode and would account for the anomalous events detected by the gridded proportional, sub-cathode assembly (Section 5.3). Moreover, they define the energy extent of the tail associated with the ^{18}O group, i.e. events within Window I of Figure 10. The extent of the tail, as limits appropriate to the various electrodes for all normal events are imposed, is summarized in Table 1.

Table 1

Energy tailing of the ^{18}O group

WINDOW	$\sum_{0}^{0.97E_T}$ (%)	Low Channel (%E_T)
ΔE_1	496 (0.23)	26 (3)
$\Delta E_1+\Delta E_2$	406 (0.18)	396 (42)
$\Delta E_1+\Delta E_2+\Delta E_3$	306 (0.14)	618 (66)
$\Delta E_1+\Delta E_2+\Delta E_3+\Delta E^*_{max}$	296 (0.13)	721 (77)
$\Delta E_1+\Delta E_2+\Delta E_3+\Delta E^*_{max}+E_R>0$	219 (0.10)	767 (82)
$\Delta E_1+\Delta E_2+\Delta E_3+\Delta E^*_{max}+E_R$	107 (0.05)	864 (92.5)

* Window I.

The results for ^{36}S ions exhibited the same general features as those for ^{18}O ions except that some anomalous total energy capture events were apparent in the ΔE_1 and ΔE_2 distributions, presumably reflecting the larger Rutherford cross-sections for ^{36}S ions scattering from carbon. The detector was operated at 120 torr so that the ^{36}S ions stopped just beyond E_R. Data from the ΔE_{max} and E_R electrodes and E_T are shown in Figure 12. A larger proportion scatter under ΔE_{max} and yield the full energy (~0.1% compared with ~0.03% for ^{18}O) though a few of these scattering events do result in a small energy degradation.

In AMS measurements of ^{36}Cl, backgrounds from anomalous ^{36}S events are not a serious problem. The resolution obtained for the ΔE_2 signal from the present detector provides essentially complete separation between S and Cl ions. Thus backgrounds in the extracted spectra of chlorine ions, due to anomalous ^{36}S events, can only originate from scattering events under the ΔE_1 and ΔE_2 electrodes. Even then, only events without significant energy degradation, but with a reduced E_R signal, can mimic the response of a ^{36}Cl ion (see Figure 3). Few such events were evident in the data of Figure 12 and most were rejected by imposing ΔE_3 limits appropriate to Cl ions so that the role of an additional ΔE_{max} electrode is a minor one. Generally, ^{35}Cl ions are not observed since the HCl^- ion is not formed. If they were present, their energy would be only 2.8% higher than that of the ^{36}Cl ions and hydrogen-scattered events would therefore pose problems similar to those reported for ^{10}Be measurements[4].

6.2 Measurements with the normal entry focal plane detector

An anode electrode structure, comprising three elements of widths 2.0, 2.8 and 2.4 cm respectively between the P_2 and P_3 sensing elements, was used. Since the data acquisition interface could only accept 6 analog inputs, the ΔE_1 and ΔE_2 electrodes were connected together to provide a single ΔE measurement while the 2.8 cm and the 2.4 cm electrodes were used to derive ΔE_{max} and E_R signals.

Measurements were made with 70 MeV ^{16}O ions, scattered at 10° from a thin gold target, for a range of detector gas pressures. The results for 175 torr, sufficient to stop the ions under E_R, and 150 torr, when the ions penetrated beyond E_R to just reach the back wall, are shown in Figure 13.

The overall features of Fig.13 are similar to those obtained with the AMS detector in Section 6.1. Several differences between the 150 and 175 torr measurements are noteworthy. At 175 torr, some ions scatter under

ΔE_{max} and the full energy is deposited (events without E_R in Fig 13(i)) whereas no such events occur at 150 torr. More energy-degraded events arise from scattering under E_R at 150 torr than do at the higher pressure. These differences are qualitatively consistent with the ^{16}O energies under the particular electrodes and the energy variation of the scattering cross-section.

Two further sets of measurements made with the detector provided strong evidence to support the proposed origins of the various types of energy-degraded events. Firstly, these involved a comparison under identical conditions of the energy-degraded events observed with isobutane (Figure 14(a)) and Freon-14 (CF_4)-(Figure 14(b)). Events attributed to hydrogen scattering, characterized by generally larger than normal ΔE_{max} values, were not evident with Freon-14. On the other hand, the components attributed to large-angle scattering under ΔE_{max} and E_R were enhanced, consistent with the increased number of heavy scattering atoms per unit volume (a factor of 1.25) and the higher average atomic number (a factor of 1.4). The observed ratio of ~3 is larger than the product of these factors, reflecting the fact that the energy of ions reaching ΔE_{max} was lower for Freon-14 than for isobutane. For both gases, the total number of scattering events yielding essentially the full ion energy (i.e. the vertical tail of ΔE_{max}) was comparable to the number of energy degraded events produced under both ΔE_{max} and E_R by large-angle scattering (other tails).

Secondly, the dependence of the fraction of energy-degraded events on detector height was determined. Lowering the detector by 4 mm, so that the incident ions were closer to the upper grid defining the cathode region, caused a dramatic increase of the fraction from $<2\times10^{-4}$ to $\sim10\times10^{-3}$ (Figure 14(c)). It was necessary to raise the detector by 8 mm to achieve an effect of the same magnitude due to scattering into the cathode. In the latter

case though, scattering from the edge of the window support was also evident. The differences can be attributed to the fact that the cathode is located 5 mm below the edge of the window whereas the lower grid is only 2 mm above the upper edge (the cathode/grid spacing is 24mm). The intensity of hydrogen-scattered events did not show any significant variation as the detector height was changed.

For the extreme positions of the detector, structure was apparent in ΔE_{max} and E_T for the energy-degraded events but was most pronounced in E_R. The pulse height distribution of E_R for the data of Fig.14(c) is shown in Fig.15. Scattering into individual grid wires is resolved, the number of peaks seen being a function of gas pressure, i.e. how far the ions penetrated into the region under the E_R electrode.

In summary, the results for both detectors confirm that most energy-degraded events can be accounted for by either hydrogen scattering for which the energy of recoiling proton is lost or from relatively large angle scattering by carbon (or fluorine) in which either the primary ion or the recoil strikes the cathode or the grid wires. Thus for carbon scattering under ΔE_{max}, energy-degraded events are distributed between total energies of E_1, the energy deposited by primary ions reaching the electrode and E_2, the energy deposited by primary ions reaching E_A (Fig.16). Similar scattering events under E_R are likewise distributed between E_2 and E_0, but with normal ΔE_{max} values. Hydrogen-scattered events are closely related to the response for lower energy ions entering the detector, the departure of events from the response curve and the energy extent of them depending on where the scattering occurs. Thus scattering by the mylar entrance window will produce events on the response curve with the greatest energy span (~20% E_0). Scattering farther into the detector produces events below the curve as is evident in Fig.16 where the calculated distribution of events

scattering midway under ΔE_{max} is indicated.

Though some scattering events under ΔE_{max} lead to premature capture of the total primary ion energy, there will also be similar scatterings that have larger than normal ΔE_{max} values but with reduced E_T values. It would be anticipated that most of these events would be confined within the hatched region indicated in Figure 16 and this expectation is borne out by the results shown in Fig.14(c). Such events constitute the only significant background which cannot be distinguished by means of a ΔE_{max} measurement. Since their intensity should be greater for Freon-14 (the measurements do not provide adequate statistical evidence), isobutane would appear to be the better gas, so far as energy-degraded backgrounds are concerned, even though hydrogen scattering does occur.

It is to be noted that events of the type observed with the AMS detector, for which it appeared that carbon scattering under ΔE_{max} yielded energy-degraded events with a slightly lower than normal ΔE_{max} value, were not evident with the focal plane detector. The difference probably stems from the narrower ΔE_{max} and E_R electrodes used in the AMS detector.

6.3 Application to reaction measurements

The results presented in Section 6.2 at 150 torr relate directly to the now familiar problem of resolving energy-degraded ^{17}O ions from ^{20}N. For such a measurement with the focal plane detector configuration described above, the ^{20}N ions should stop under E_R; the extent to which they penetrate determining the dynamic range of ^{20}N energies accepted. With magnetic rigidities about equal to the highest ^{20}N energy, ^{17}O ions would penetrate beyond E_R, but still be stopped. Normally behaved ^{17}O ions within this rigidity range and beyond would produce a P_3 signal and could thus be rejected. Accordingly, the results for ^{16}O at 70 MeV provide an indication

of likely ^{17}O behaviour since the stopping conditions are similar.

For reaction data, a range of ion energies is involved but it is possible, and more straightforward to consider a limited range of magnetic rigidity. The calculated ΔE_{max} and E_R signals for 109 MeV ^{17}O ions, which have the same rigidity as 92.6 MeV ^{20}N ions, are shown in Figure 17. The gas pressure used for the calculations was sufficient to stop ^{20}N ions, with energies between 84 and 93 MeV, under E_R. For the experimental conditions envisaged (see Section 7), the maximum expected ^{20}N energy is ~ 91 MeV so that the most critical background affecting the determination of the highest ^{20}N energy produced is that between E_T values corresponding to incident ^{20}N energies between 91 and at least 93 MeV.

On the basis of the results presented in Sections 6.1 and 6.2, the anomalous events shown in Figure 17 are:

(a) hydrogen scattering events before ΔE_{max} that follow the locus appropriate to lower energy ^{17}O ions incident on the detector

(b) scattering events under E_R which have a ΔE_{max} value appropriate to 109 MeV ^{17}O

(c) hydrogen scattering events occurring mid-way under the ΔE_{max} electrode and three quarters of the distance under the electrode.

Events of types (a) and (b) are well separated relative to the observed resolutions, from the critical region above the calculated position for 93 MeV ^{20}N ions. Type (c) events in the region can only arise from scatterings in which the proton recoil energy is less than 10 MeV. Thus such events will have measured E_T values within 10 MeV of the value for

normally-behaved ^{17}O ions, i.e. above 93.6 MeV. Since the E_T value of 93 MeV ^{20}N ions is 88.30 MeV, the type (c) scattering events should be readily distinguished by means of the dependence of E_T with position along the detector. In other words, when identification is based on m/q^2 values calculated from $(B_\rho)^2/E$, energy-degraded events from hydrogen scattering of ^{17}O result in values well-removed from the ^{20}N value. Anomalous events not shown in Figure 14 are those for which the correct E_T is measured because of scattering under ΔE_{max} or E_R and those corresponding to energy-degraded scatterings from carbon under ΔE_{max}. The former pose no problem because they would be identified correctly as ^{17}O ions and the latter would result in ΔE_{max} values comparable or lower than the ^{17}O value and generally would have no E_R signal.

One source of energy-degraded events remains, viz the relatively large-angle scattering under ΔE_{max} causing larger than normal ΔE_{max} values (Sect.6.2). Partial discrimination of these can be achieved by selecting only the events which have the correct dependence of ΔE_{max} with magnetic rigidity and with E_R.

The behaviour for a range of rigidities can also be predicted from Figure 17. For both lower and higher magnetic rigidities, hydrogen scattering under ΔE_{max} can produce events with ΔE_{max} and E_R values which correspond to higher energy ^{20}N ions, but again these can be distinguished by E_T values uncorrelated with position, i.e. by m/q^2. Carbon scattering of lower rigidities under E_R (and events due to reactions under ΔE_{max}) can be eliminated by ensuring that the position dependences of both ΔE_{max} and E_R are appropriate to ^{20}N ions.

The electrode configuration is considered to be close to the optimum. The width of ΔE_{max} was chosen to maintain almost the maximum possible difference between ^{17}O and ^{20}N ions while ensuring good resolution for the

ΔE_{max} measurement. If the width were reduced, by extending the un-used 2 cm long section, the low energy extent of the energy-degraded tail would not be reduced sufficiently to remove anomalous events from the critical region and the ratio of the ΔE_{max} values would increase by only ~3%. Because of the large difference in range of ^{20}N and ^{17}O ions of the same rigidity, some scattering events unidentifiable on the basis of ΔE_{max} and E_R measurement alone, will occur in the critical region regardless of electrode configuration.

7. Reaction Measurements

In order to confirm the results of the investigations using scattered ^{18}O ions, measurements were made also of the $^{48}Ca(^{18}O,^{20}N)^{46}Sc$ reaction using two electrode configurations. Isobutane was used for both measurements.

7.1 Single E_R electrode

The measurement was made at 6° with a bombarding energy of 117 MeV. At a gas pressure of 290 torr ^{17}O ions, within the same magnetic rigidity range as the ^{20}N ions of interest, stopped under the P_3 element while the ^{20}N ions stopped under E_R. The E_R electrode was 3.5 cm wide and located immediately prior to the P_3 sensing element. Six linear signals E_T, P_1, ΔE_1, ΔE_2, P_2 and E_R were recorded for each event along with logic signals to flag the occurrence of pile-up, a pulse from the gridded proportional counter below the cathode or a veto (P_3) signal.

The results, showing the distribution of E_T and E_R values for events within a narrow range of magnetic rigidity and with ΔE_1 and ΔE_2 values corresponding to ^{20}N ions are given in Figure 18. As expected, the energy-degraded events have a locus beyond the normal E_R events and contribute a

small, but significant, background beyond the events believed to be due to ^{20}N ions. The rejection of energy-degraded events, provided almost entirely by approximately equal numbers of the veto and gridded proportional counter flags, is substantial but inadequate.

7.2 Multiple E_R electrode

The measurement of Section 7.1 was repeated under identical conditions except that the signals ΔE_{max} and E_R were obtained from the divided rear anode electrode (Section 6.2) and the ΔE_1 and ΔE_2 electrodes were coupled to provide a single ΔE measurement. The sub-cathode gridded proportional counter was not used.

Two representations of the results illustrate the effectiveness of the ΔE_{max} electrode. In Fig.19, the distribution of E_T values as a function of P_2 is shown for events within a range of m/q^2 values including that of $^{20}N^{7+}$ and for the appropriate values of $(B\rho)^2.\Delta E$ (used instead of $E.\Delta E$ since many of the ion species present were not stopped). The detector was positioned so that the focal plane for the $^{48}Ca(^{18}O,^{20}N)^{46}Sc$ reaction intersected the P_2 element at a position corresponding approximately to that expected for the ground state group (~channel 2320 in Fig.19).

Random events span the region, defined by reference to the adjacent species $^{16}N6^+$, in which ^{20}N ions would be expected. However, the corresponding ΔE_{max} data, for the same $(B\rho)^2$ ΔE values and for an m/q^2 range about 50% larger than that of the ^{20}N region indicated in Fig.19, appear to be background free (Fig.20). The small, but significant, background beyond the ground state has been eliminated. The measurement of ΔE_{max} allows identification of two sources of background, viz. some $^{18}O^{7+}$ events at low rigidity and the anticipated $^{17}O^{7+}$ events, which have an intensity distribution along the detector consistent with the spectrum shown in

Fig.19. The former are attributed to leakage from the very intense $^{18}O^{7+}$ group at a higher $(B\rho)^2.\Delta E$ value.

8. Summary

It has been demonstrated that the majority of energy-degraded events observed with gas ionization detectors can be accounted for in terms of scattering by the stopping gas.

An electrode configuration that provides detailed energy loss information near the end of the range of each ion, where the scattering is most likely, has been shown to enable identification and rejection of most of the scattering events. As a result, the quality of measurement of a very low cross-section reaction has been improved significantly.

Although scattering effects from both hydrogen and carbon are evident with isobutane, its use with ionization detectors is preferable to other stopping gases for reaction measurements where energy-degraded events are likely to be troublesome. However, background problems observed in gas detectors used for accelerator mass spectrometry are more likely to stem from hydrogen scattering. Accordingly, stopping gases not containing hydrogen (e.g. Freon-14) should be used.

References

[1] H.W. Fulbright and J.R. Erskine, Nucl. Inst. and Meth. 162 (1979) 355.

[2] L.K. Fifield, J.R. Durell, M.A.C. Hotchkis, J.R. Leigh, T.R. Ophel and D.C. Weisser, Nucl. Phys. A385 (1982) 505.

[3] Annual Report, Department of Nuclear Physics, ANU; P/852 (unpublished, 1982).

[4] C. Tuniz, R.K. Moniot, W. Savin, S. Vajda, T.H. Kruse, D.K. Pal, G.F. Herzog and M.J. Carr, Nucl. Inst. and Meth. B5 (1984) 321.

[5] T.R. Ophel, "Aspects of focal plane detectors", ANU Report P/848 (unpublished, 1982).

[6] J. A. Kushner, R.H. Spear, W.J. Vermeer, M.T. Esat, A.M. Baxter and S. Hinds, Physics Letters 115B (1982) 437.

[7] "SHEBA - a proposal for updating the ANU accelerator" (unpublished, 1984); W.R. Phillips (private communication).

[8] M.A.C. Hotchkis, ANU thesis (unpublished, 1984); C.L. Woods, W.N. Catford, N.A. Orr and R.B. Sadlier, Nucl. Phys. A476 (1988) 392.

[9] P.V. Drumm, SERC Laboratory, Daresbury (private communication) K.E. Rehm, Argonne National Laboratory (private communication). See also reference 5).

[10] T.R. Ophel and A. Johnston, Nucl. Inst. and Meth. 157 (1978) 461.

[11] L.K. Fifield, T.R. Ophel, J.R. Bird, G.E. Calf, G.B. Allison and A.R. Chivas, Nucl. Instr. and Meth. B29 (1987) 114.

[12] G. Rosner, B. Heck, J. Pochodzalla, G. Hlawatsch, B. Kolb and A. Miczaika, Nucl Inst and Meth. 188 (1981) 561.

[13] D.F. Measday and C. Richard-Serre, Nucl. Inst. & Meth. 76 (1969) 45.

[14] T.R. King, J.J. Krausmaar, R.A. Ristenen, R. Smythe & D.M. Stupin, Nucl. Inst & Meth. 88 (1970) 17.

[15] T.R. Ophel and I.F. Wright, Proc. Phys. Soc. 71 (1958) 389.

[16] W.M. Deuchars and G.P. Lawrence, Nature 191 (1961) 995.

[17] W. N. Catford, L.K. Fifield, M.A.C. Hotchkis, T.R. Ophel, N.A. Orr, D.C. Weisser and C.L. Woods, Nucl. Instr. and Meth. A260 (1987) 146.

[18] Annual Report, Department of Nuclear Physics, ANU; P/880 (unpublished, 1983).

[19] J.R. Erskine, T.H. Braid and J.C. Stolzfus, Nucl. Instr. and Meth. 135 (1976) 67.

Figure Captions

Figure 1. Portion of the data obtained during an attempted measurement of the mass of ^{20}N. Energy tailing of the intense ^{18}O ions is very evident; that from the lower intensity ^{17}O ions is less obvious, but nonetheless causes a background in the extracted momentum distribution of the ^{20}N ions. The detector used is described in ref. 10.

Figure 2. Schematic representation of focal plane detector data. The upper section illustrates the typical low level background sources, as a function of measured energy and portion, for several charge states of one ion species in the detector. The lower section indicates the effect of these backgrounds on the separation of ion species (all with the same charge state q).

Figure 3. An accelerator mass spectrometry measurement of ^{36}Cl obtained with a small ionization detector. Correlated energy-degraded tail events (<0.1% of total intensity) associated with both the ^{36}S and ^{37}Cl groups are evident. (Each point corresponds to one or more counts).

Figure 4. Pulse height distributions measured with the bottom half of the sawtooth for events in the ^{36}S group and in the tail.

Figure 5. Section view of a focal plane detector designed for mounting such that incident ions enter normally. The cathode is gridded (125μm diameter gold-plated tungsten wires with a 2 mm spacing). Several sub-cathode electrodes were investigated (see text). The final electrode configuration described in Section 6.2 is shown. For some measurements, the ΔE_1 electrode was divided to provide ΔE_1 and ΔE_2 signals.

Figure 6. Variation of P_3 efficiency and the pulse heights of E_T and E_R with gas pressure. Calculated values for E_T and E_R are also shown.

Figure 7. Contour representation of the residual energy and the total energy for 69.7 MeV ^{16}O ions at a gas pressure slightly below that required to stop the ions beneath the E_R electrode. (Each point corresponds to 1 or more counts).

Figure 8. Contour representations of the same data shown in Figure 7 illustrating the variation of the residual energy (E_R) with ion direction (as deduced from P_1 and P_2). (Each point corresponds to 1 or more counts).

Figure 9. Schematic contour representations of the signals from the various electrodes of the AMS detector as a function of E_T for 66 MeV ^{16}O ions. The left hand column shows the data without limits imposed; the right column shows the same data as the limits corresponding to normal events for the preceding electrodes are imposed. Increasing intensity is indicated by more closely spaced hatching.

Figure 10. Contour representation of the actual data for ΔE_{mx} and E_T obtained using the AMS detector with 66 MeV ^{18}O ions. Events with ΔE_3 values beyond the normal limits or with no associated E_R signal are indicated. (Each point corresponds to 1 or more counts).

Figure 11. Contour representations of the signals from successive pairs of electrodes in the AMS detector obtained with 66 MeV ^{18}O ions (Each point corresponds to 1 or more counts).

Figure 12. Contour representations of $\Delta E_{max}/E_T$ and $E_R/\Delta E_{max}$ obtained with 132 MeV ^{36}S ions. All of the data shown are associated with ΔE_1, ΔE_2 and ΔE_3 values within the limits appropriate to normally behaved ^{36}S ions. (Each point corresponds to 1 or more counts).

Figure 13. Results obtained for 70 MeV ^{18}O ions using the normal entry focal plane detector at gas pressures of 175 torr (left column) and 150 torr (right column). Contour representations of $\Delta E_{max}/E_T$, $E_R/\Delta E_{max}$ and E_R/E_T are shown and the origins of the various anomalous events are indicated. (Each point corresponds to 1 or more counts).

Figure 14. Contour representations of $\Delta E_{max}/E_T$ obtained for 70 MeV ^{18}O ions scattered from Au at 10°. The results for isobutane and Freon-14 are shown in (a) and (b). The effect of lowering the detector is shown in (c) - (see text). (Each point corresponds to 1 or more counts).

Figure 15. Pulse height distribution of the E_R signal obtained from the measurement of Figure 14(c).

Figure 16. Schematic summary of the characteristics of energy-degraded events from the various scattering processes.

Figure 17. Calculated response of the ΔE_{max} and E_R electrodes in the normal entry focal plane detector for 109 MeV ^{17}O and 93 MeV ^{20}N ions (see text).

Figure 18. Contour representation of E_T and E_R from a measurement of the $^{48}Ca(^{18}O,^{20}N)^{46}Sc$ reaction using only an E_R electrode. The region of the intense ^{17}O ions (removed by the P_3 veto) is indicated by the hatched area. Events marked (+) are believed to be ^{20}N ions, open circles (0) are events removed by either the gridded proportional sub-cathode detector or the P_3 veto. (Each symbol corresponds to 1 or more counts).

Figure 19. Contour representation of E_T/P_2 for a second measurement of the $^{48}Ca(^{18}O,^{20}N)^{46}Sc$ reaction. The region in which ^{20}N ions should occur is indicated, along with the $^{17}O^{7+}$ distribution along the detector.

Figure 20. Contour representation of $\Delta E_{max}/P_2$ for the data of Figure 19 (see text). (Each point corresponds to 1 or more counts.)

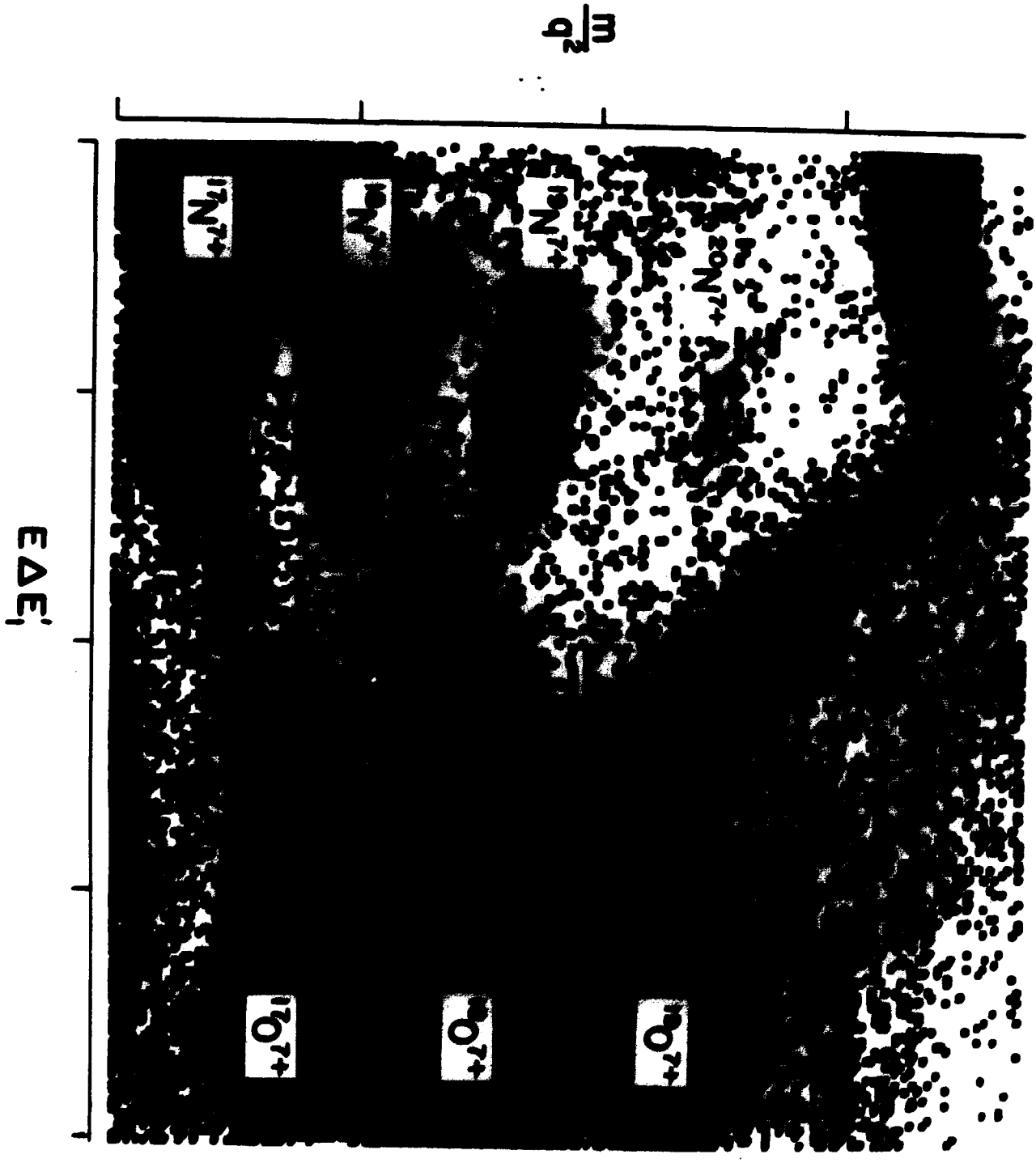

Fig. 1

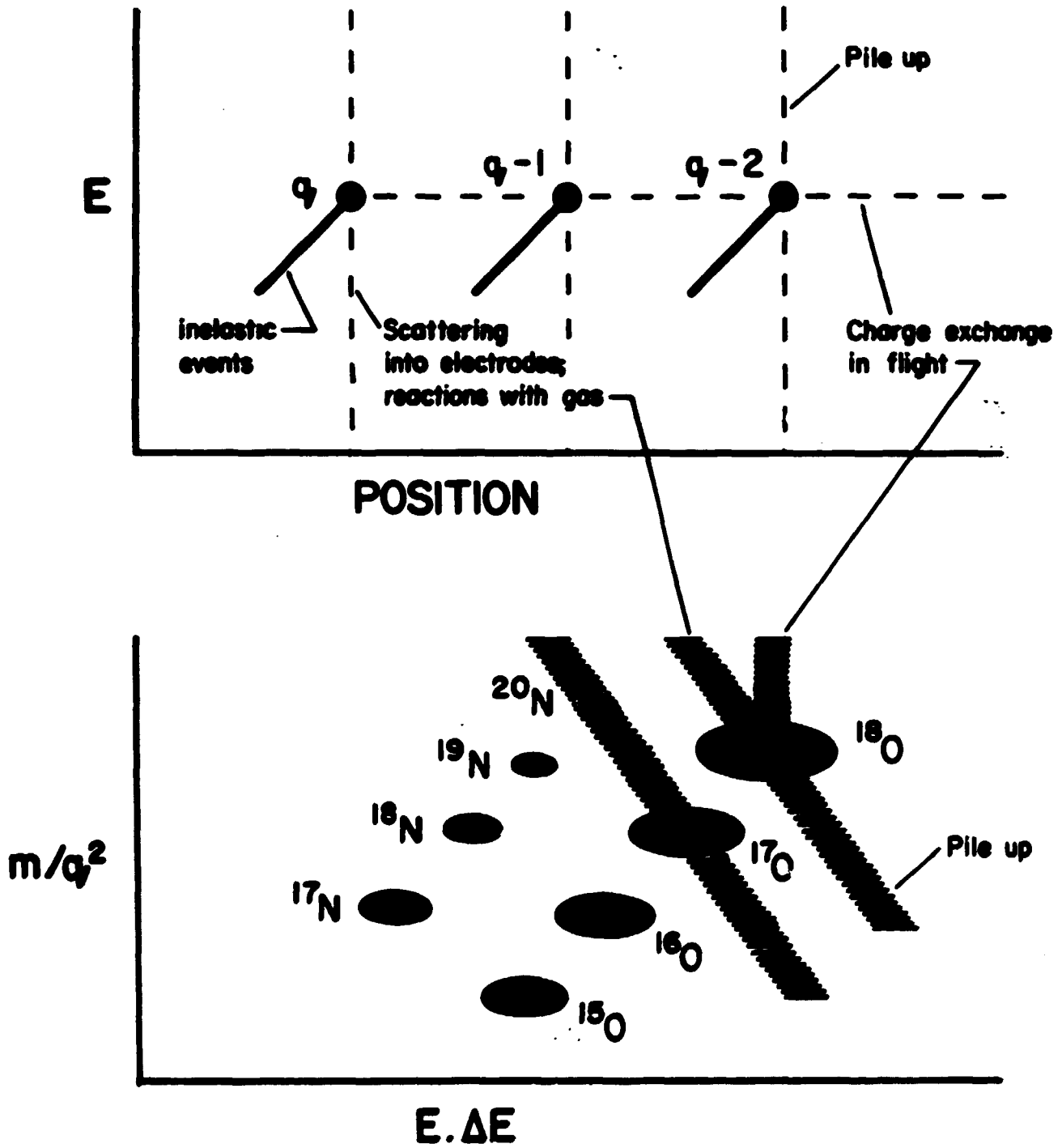
E
q
q-1
q-2
Pile up
inelastic events
Scattering into electrodes; reactions with gas
Charge exchange in flight
POSITION
m/q²
20N
19N
18N
17N
18O
17O
16O
15O
Pile up
E.ΔE

Fig. 2

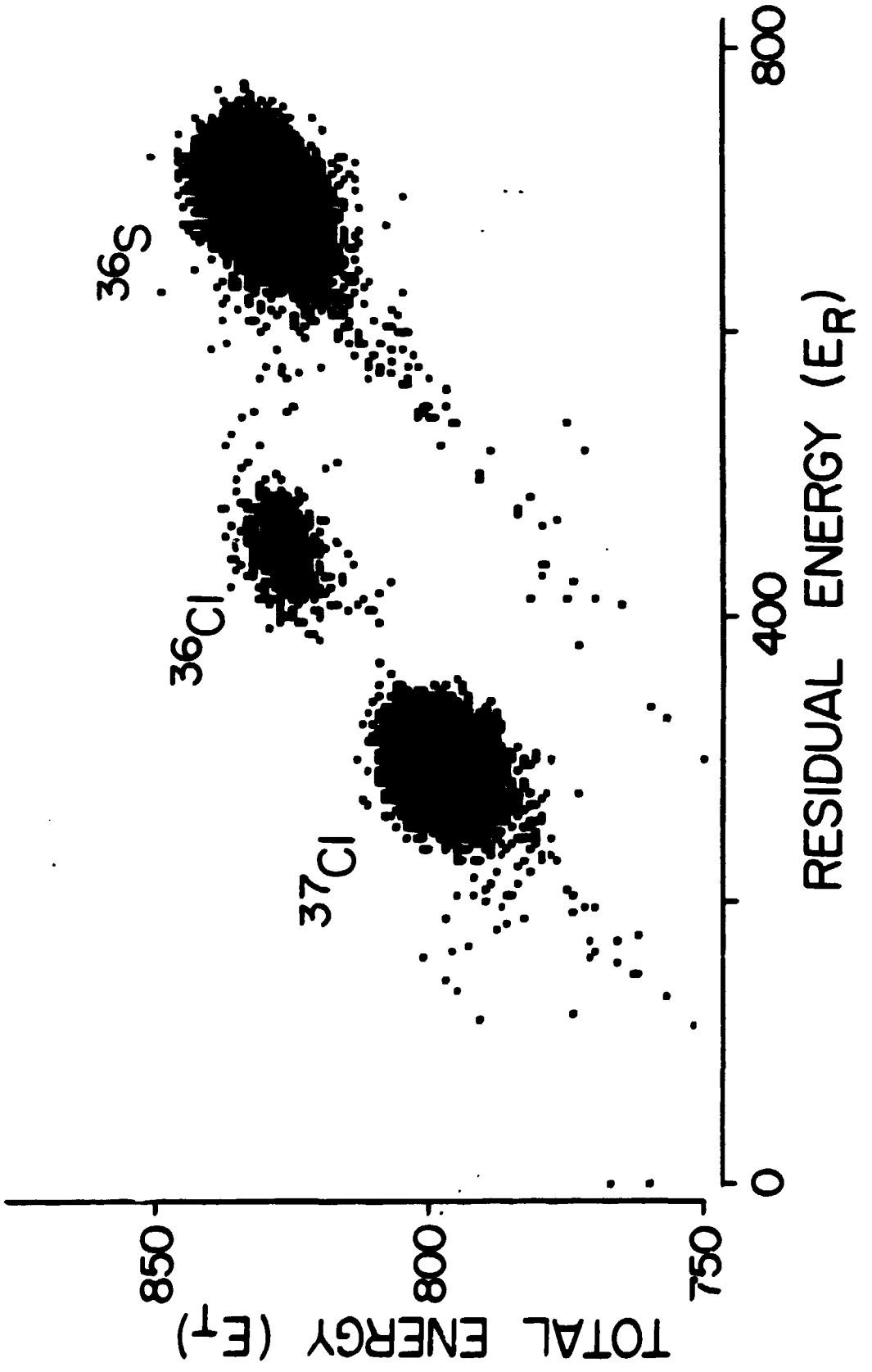
36S
36Cl
37Cl
TOTAL ENERGY (ET)
850
800
750
0
400
800
RESIDUAL ENERGY (ER)

Fig. 3

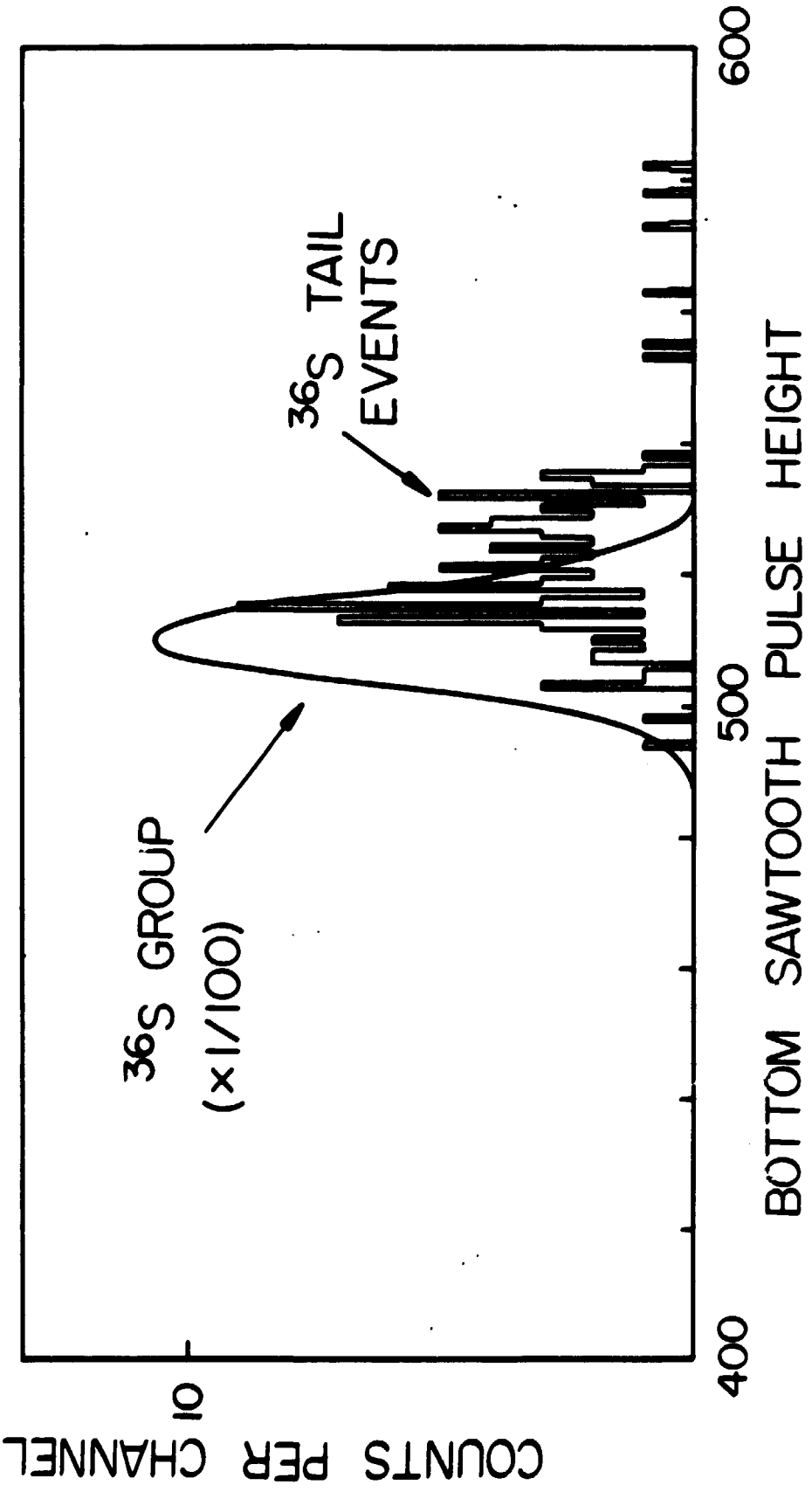
COUNTS PER CHANNEL
10
400
500
600
BOTTOM SAWTOOTH PULSE HEIGHT
^{36}S GROUP
(×1/100)
^{36}S TAIL
EVENTS

Fig. 4

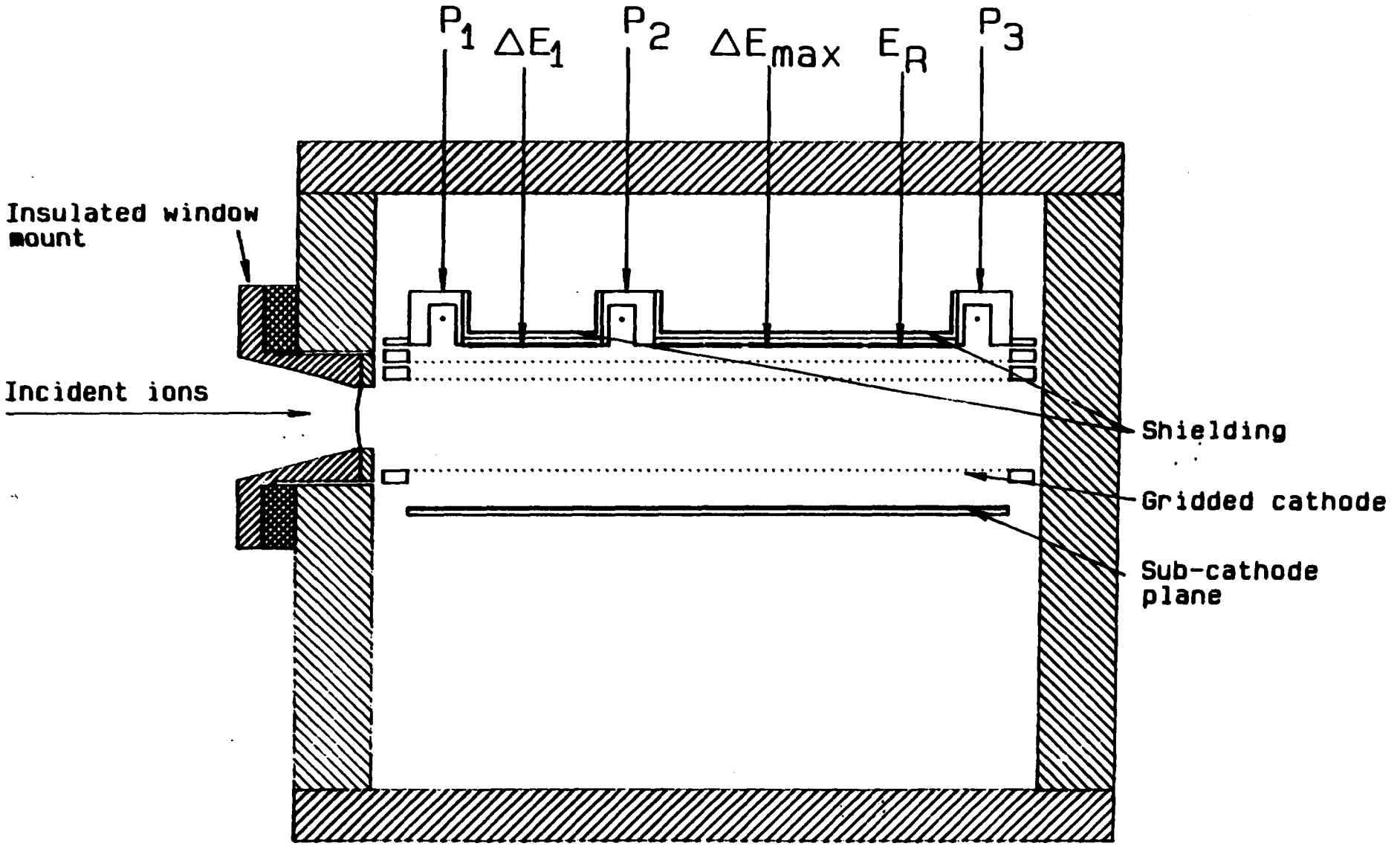
P1 ΔE1
P2 ΔEmax ER
P3
Insulated window mount
Incident ions
Shielding
Gridded cathode
Sub-cathode plane

Fig. 5

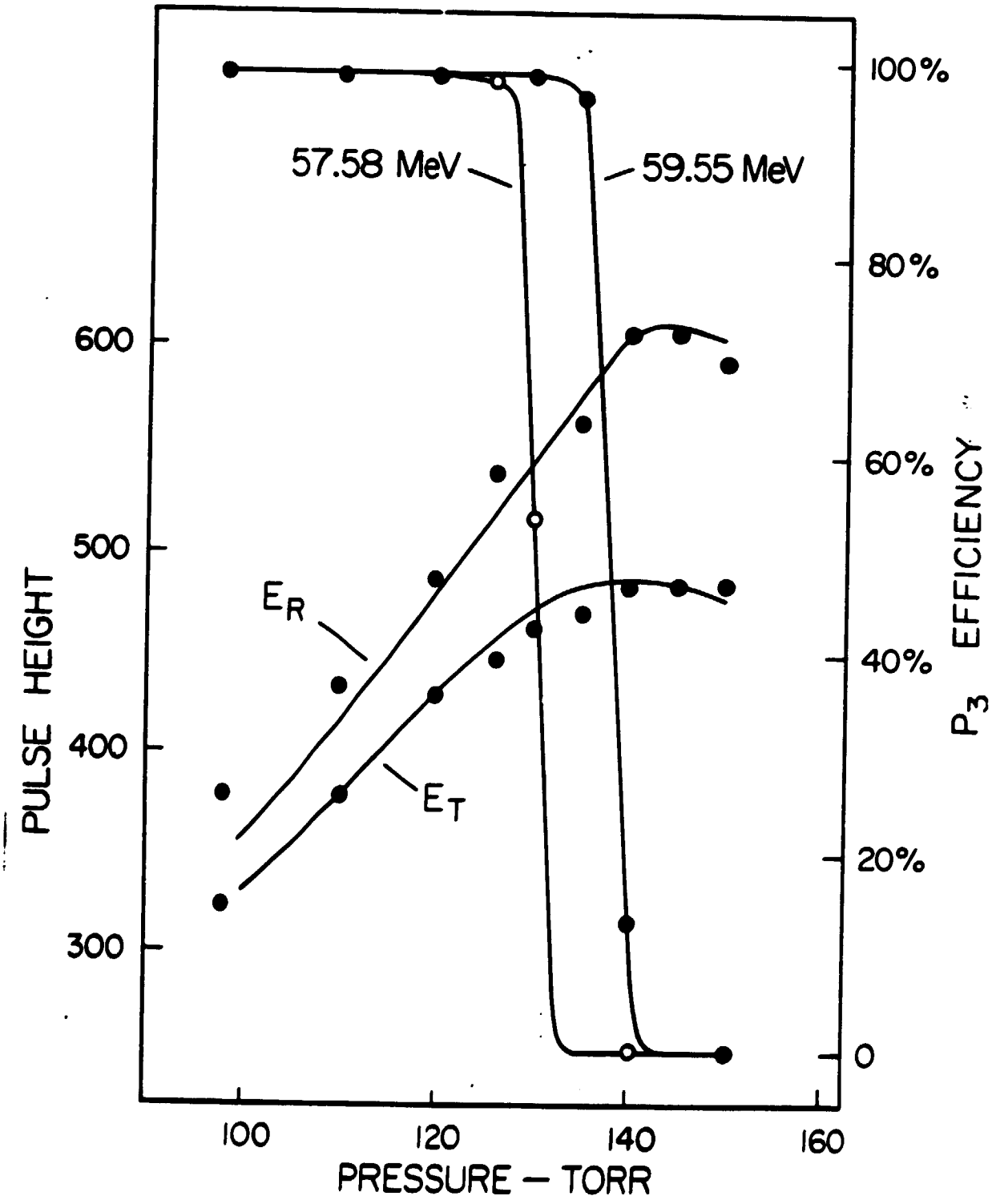
57.58 MeV
59.55 MeV
E_R
E_T
PULSE HEIGHT
600
500
400
300
100%
80%
60%
40%
20%
0
P_3 EFFICIENCY
100
120
140
160
PRESSURE — TORR

Fig. 6

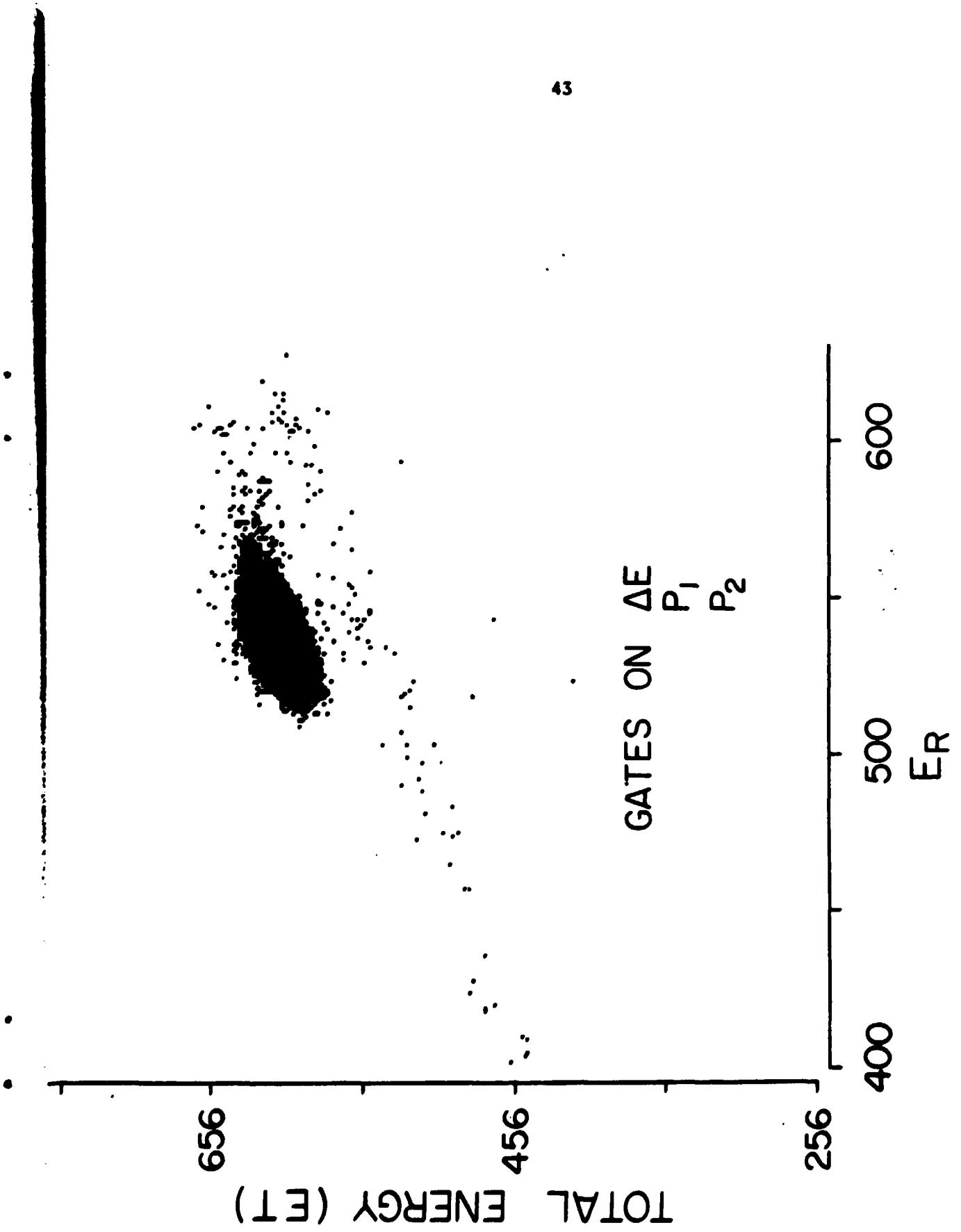

Fig. 7

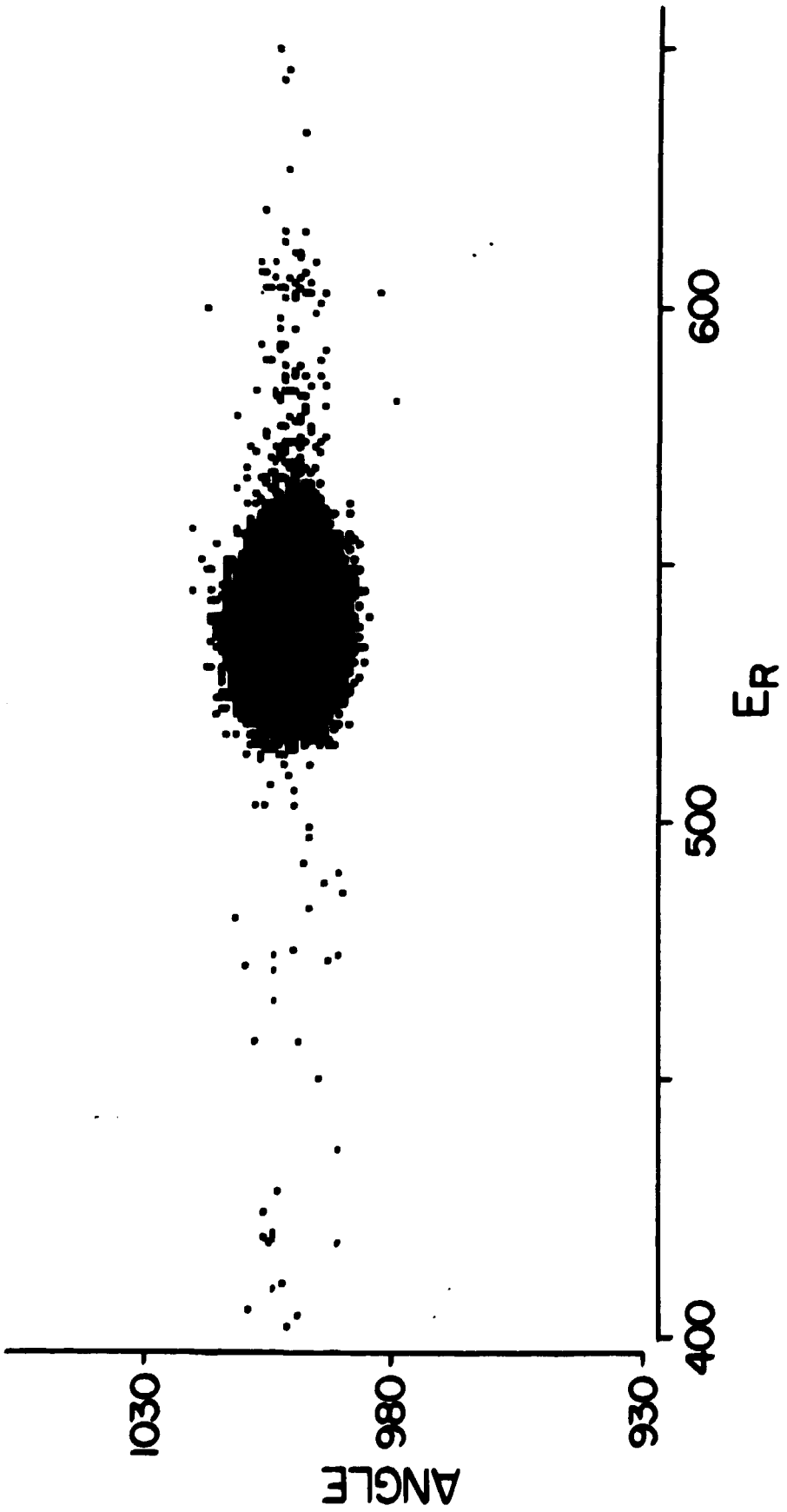

Fig. 8

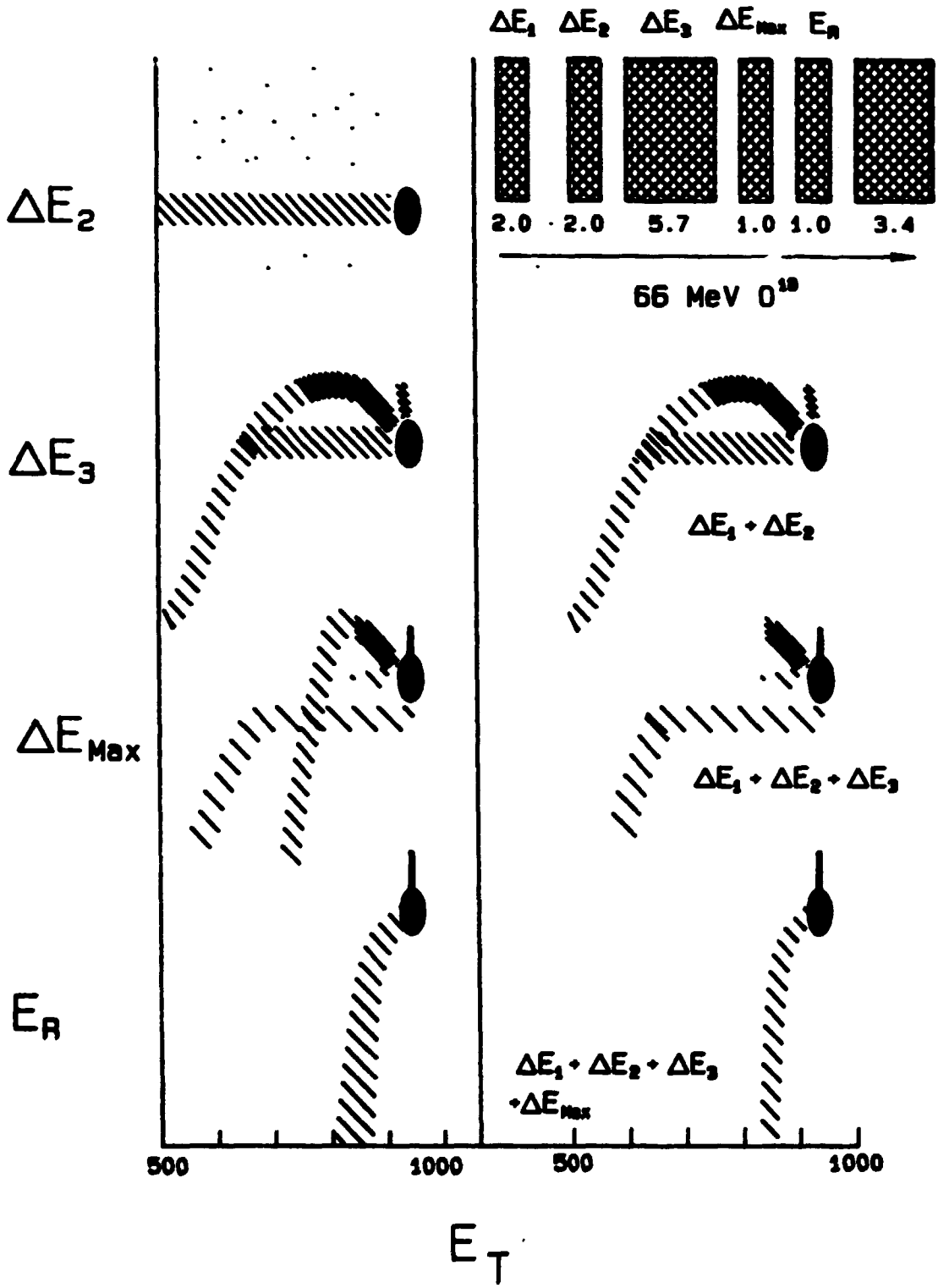
ΔE1 ΔE2 ΔE3 ΔEMax ER
2.0 2.0 5.7 1.0 1.0 3.4
66 MeV O18
ΔE2
ΔE3
ΔEMax
ER
ΔE1 + ΔE2
ΔE1 + ΔE2 + ΔE3
ΔE1 + ΔE2 + ΔE3 + ΔEMax
500
1000
500
1000
ET

Fig. 9

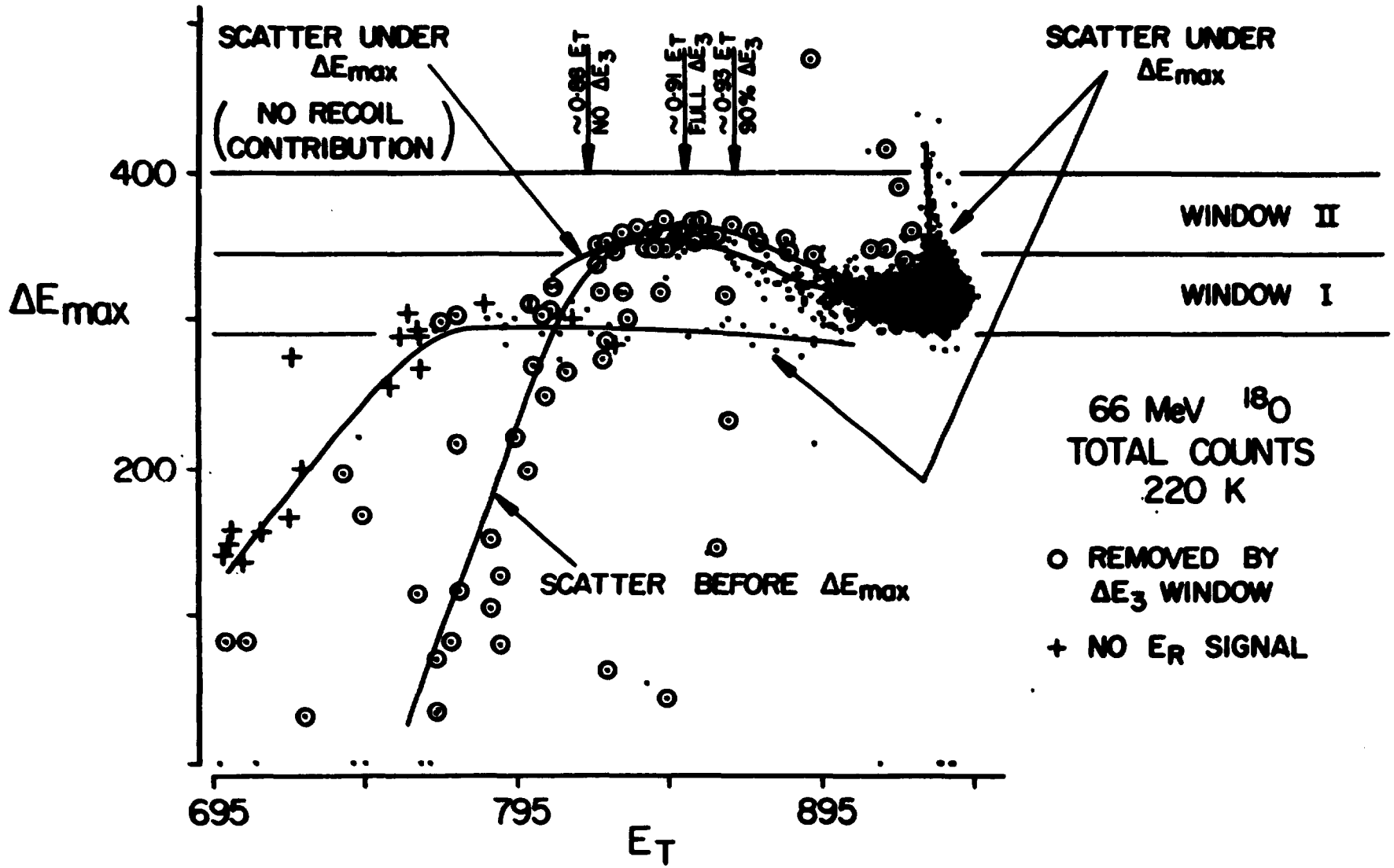
SCATTER UNDER
ΔEmax
(NO RECOIL
CONTRIBUTION)
~0.88 ET
NO ΔE3
~0.91 ET
FULL ΔE3
~0.93 ET
90% ΔE3
SCATTER UNDER
ΔEmax
400
WINDOW II
WINDOW I
ΔEmax
200
66 MeV 18O
TOTAL COUNTS
220 K
O REMOVED BY
ΔE3 WINDOW
+ NO ER SIGNAL
SCATTER BEFORE ΔEmax
695
795
895
ET

Fig. 10

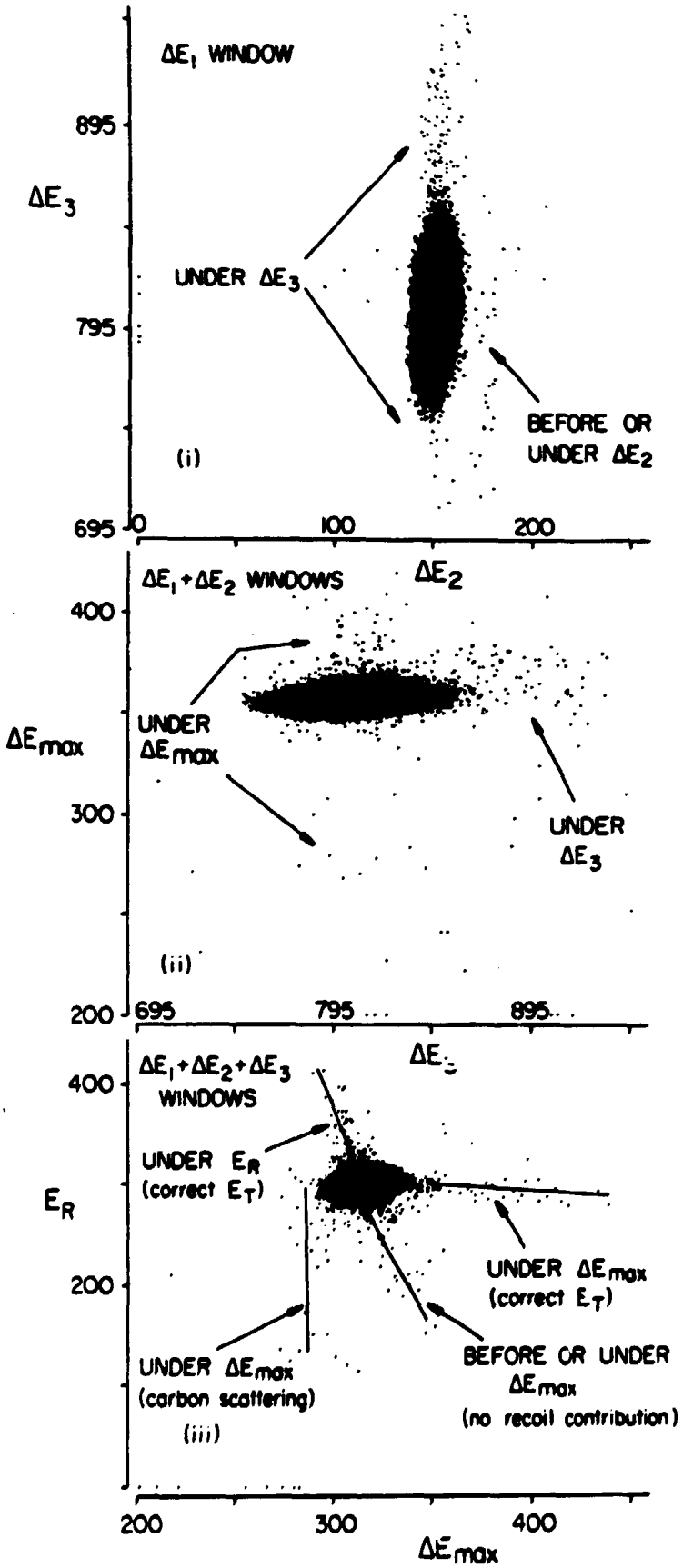
ΔE1 WINDOW
895
ΔE3
795
695
UNDER ΔE3
BEFORE OR
UNDER ΔE2
(i)
0
100
200
ΔE2
ΔE1+ΔE2 WINDOWS
400
ΔEmax
300
200
UNDER
ΔEmax
UNDER
ΔE3
(ii)
695
795
895
ΔE3
ΔE1+ΔE2+ΔE3
WINDOWS
400
UNDER ER
(correct ET)
ER
200
UNDER ΔEmax
(correct ET)
BEFORE OR UNDER
ΔEmax
(no recoil contribution)
UNDER ΔEmax
(carbon scattering)
(iii)
200
300
400
ΔEmax

Fig. 11

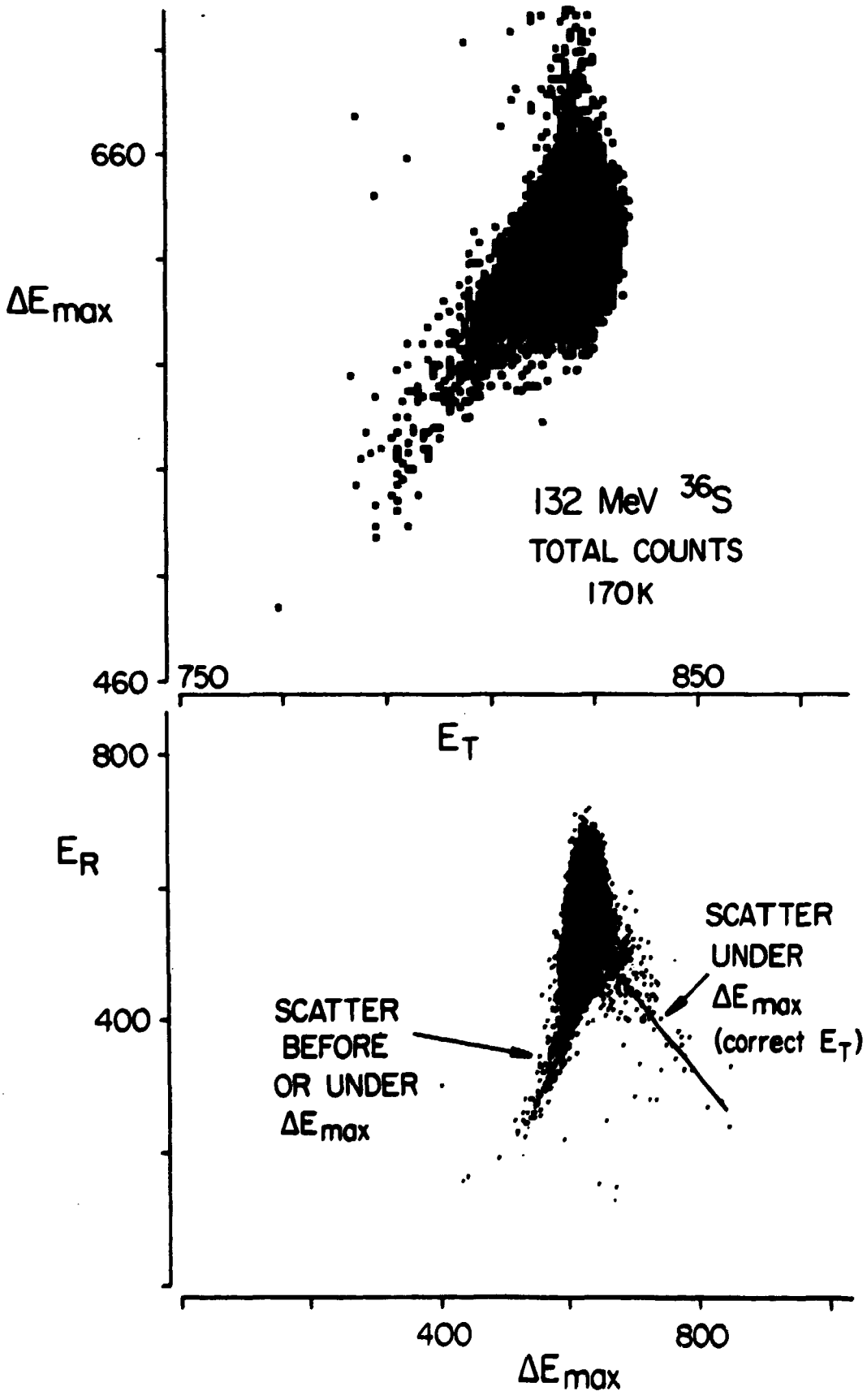
660
460
ΔE_{max}
750
850
E_T
132 MeV ^{36}S
TOTAL COUNTS
170K
800
400
E_R
SCATTER
UNDER
ΔE_{max}
(correct E_T)
SCATTER
BEFORE
OR UNDER
ΔE_{max}
400
800
ΔE_{max}

Fig. 12

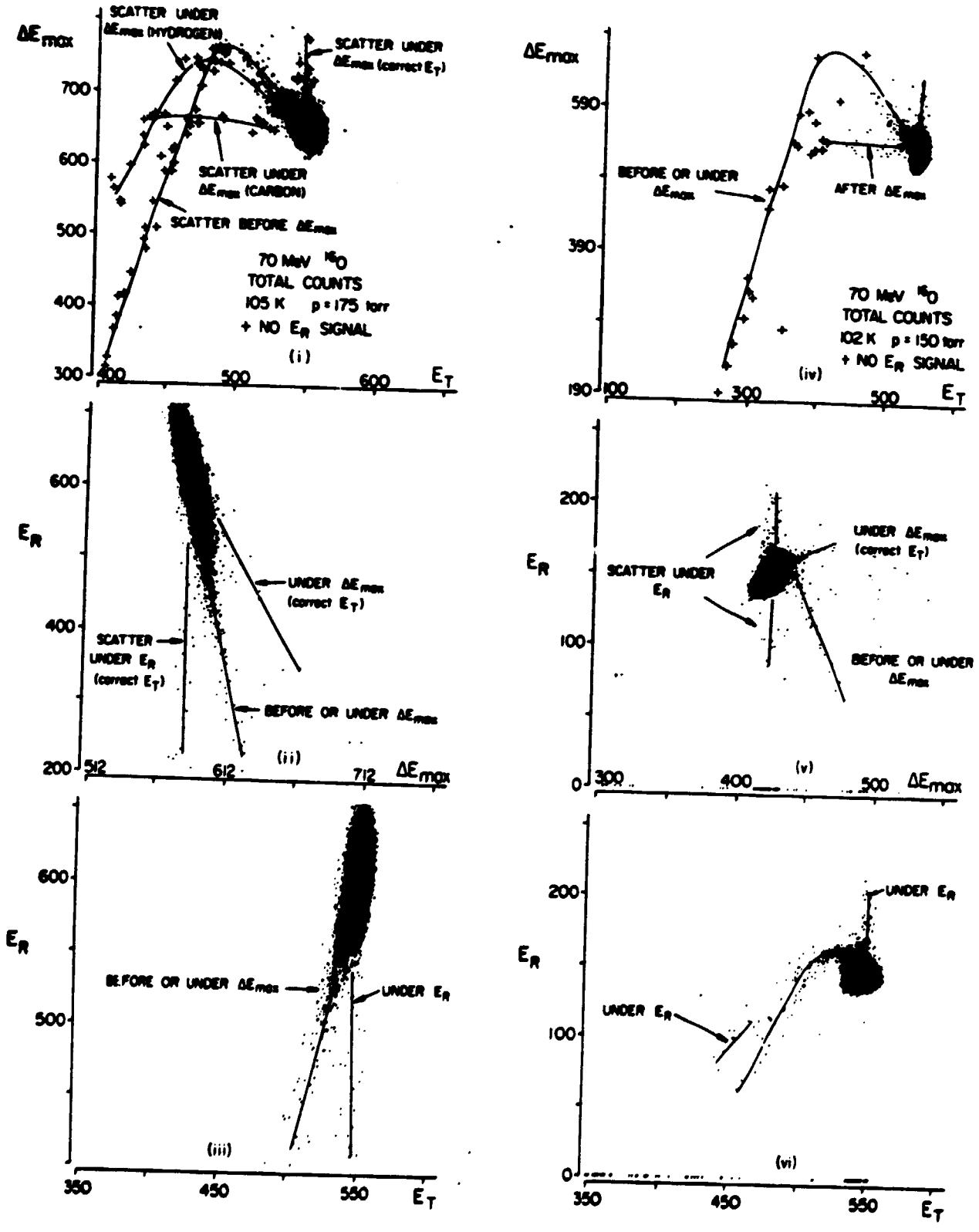
SCATTER UNDER ΔE max (HYDROGEN)
SCATTER UNDER ΔE max (correct E_T)
SCATTER UNDER ΔE max (CARBON)
SCATTER BEFORE ΔE max
70 MeV 16O
TOTAL COUNTS
105 K p = 175 torr
+ NO E_R SIGNAL
(i)
ΔE max
E_T
BEFORE OR UNDER ΔE max
AFTER ΔE max
70 MeV 16O
TOTAL COUNTS
102 K p = 150 torr
+ NO E_R SIGNAL
(iv)
E_R
UNDER ΔE max (correct E_T)
SCATTER UNDER E_R (correct E_T)
BEFORE OR UNDER ΔE max
(ii)
SCATTER UNDER E_R
UNDER ΔE max (correct E_T)
BEFORE OR UNDER ΔE max
(v)
BEFORE OR UNDER ΔE max
UNDER E_R
(iii)
UNDER E_R
UNDER E_R
(vi)

Fig. 13

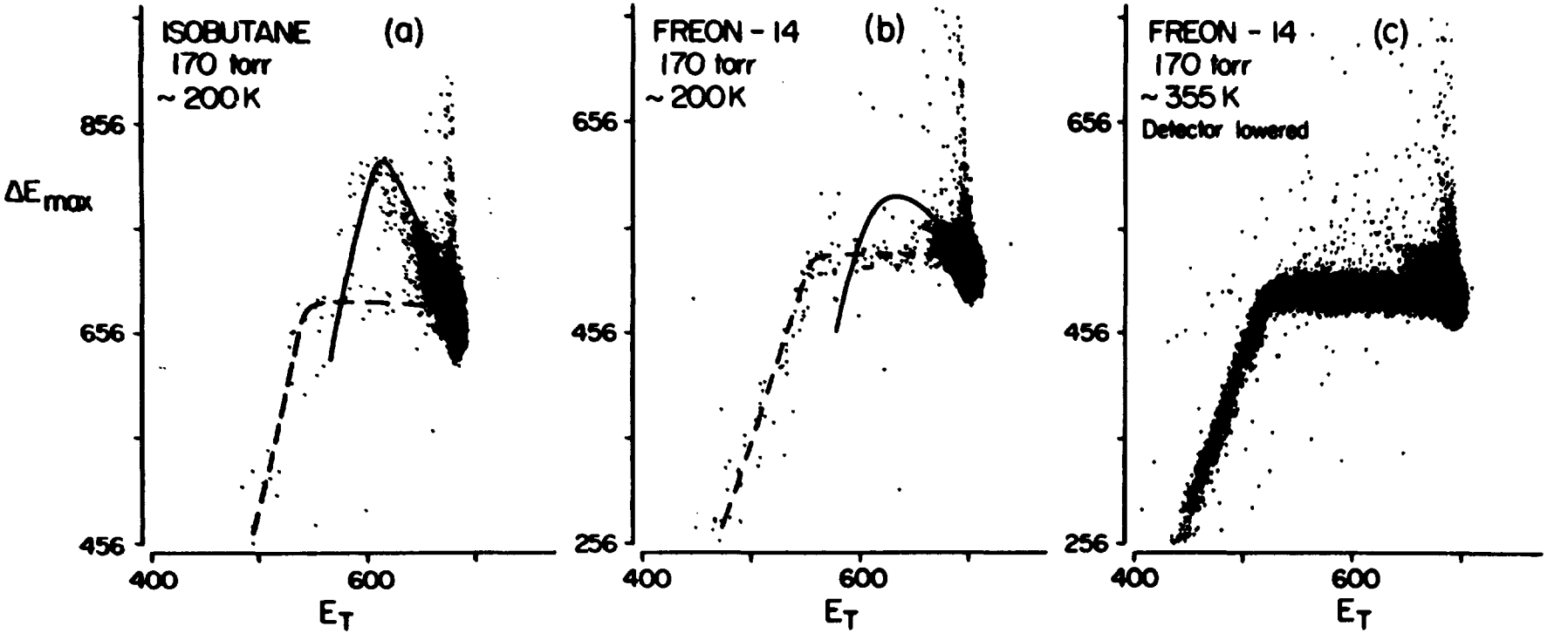
ISOBUTANE
170 torr
~ 200 K
(a)
FREON - 14
170 torr
~ 200 K
(b)
FREON - 14
170 torr
~ 355 K
Detector lowered
(c)
ΔE max
856
656
456
256
400
600
E T

Fig. 14

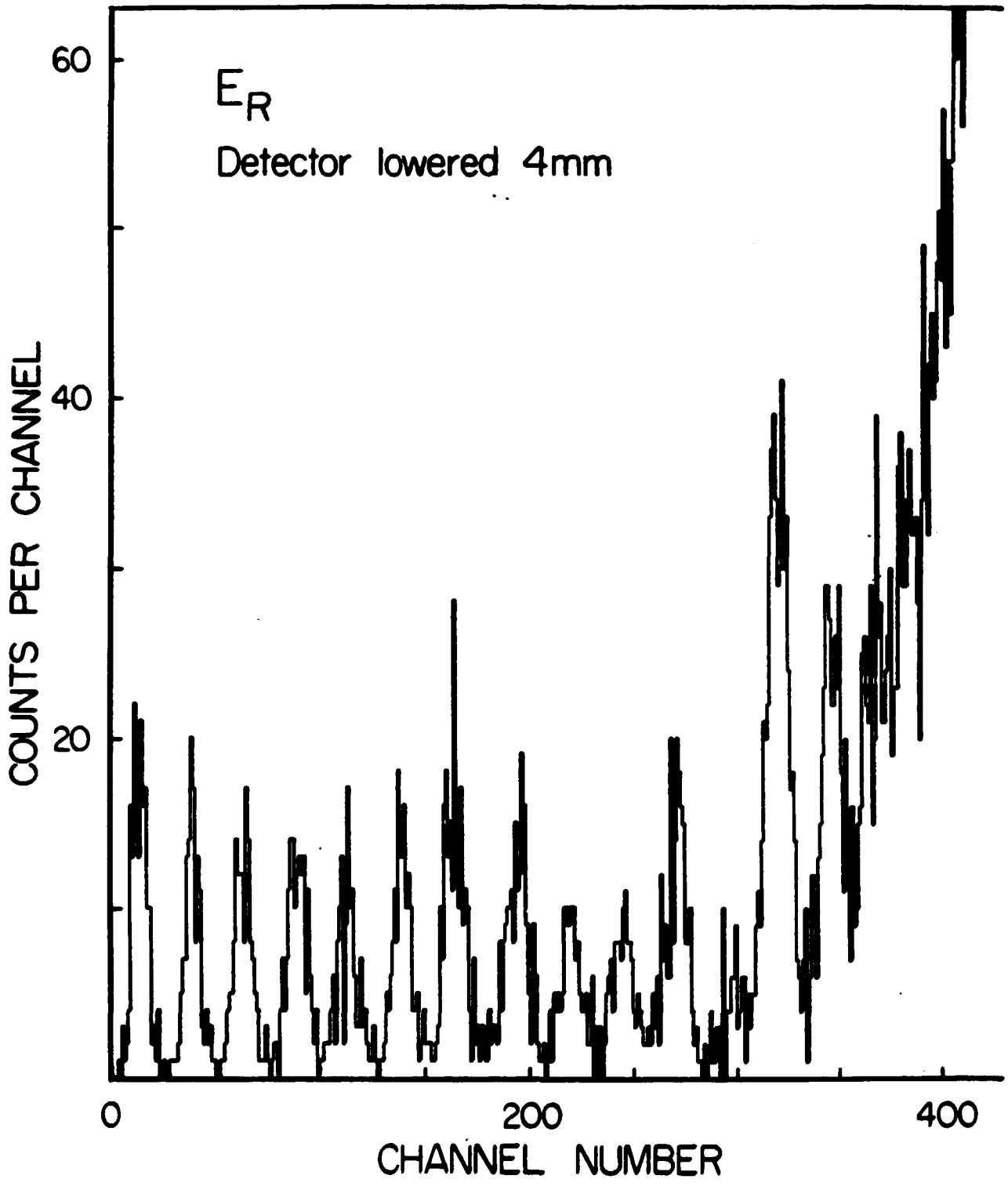
E_R
Detector lowered 4mm
COUNTS PER CHANNEL
60
40
20
0
200
400
CHANNEL NUMBER

Fig. 15

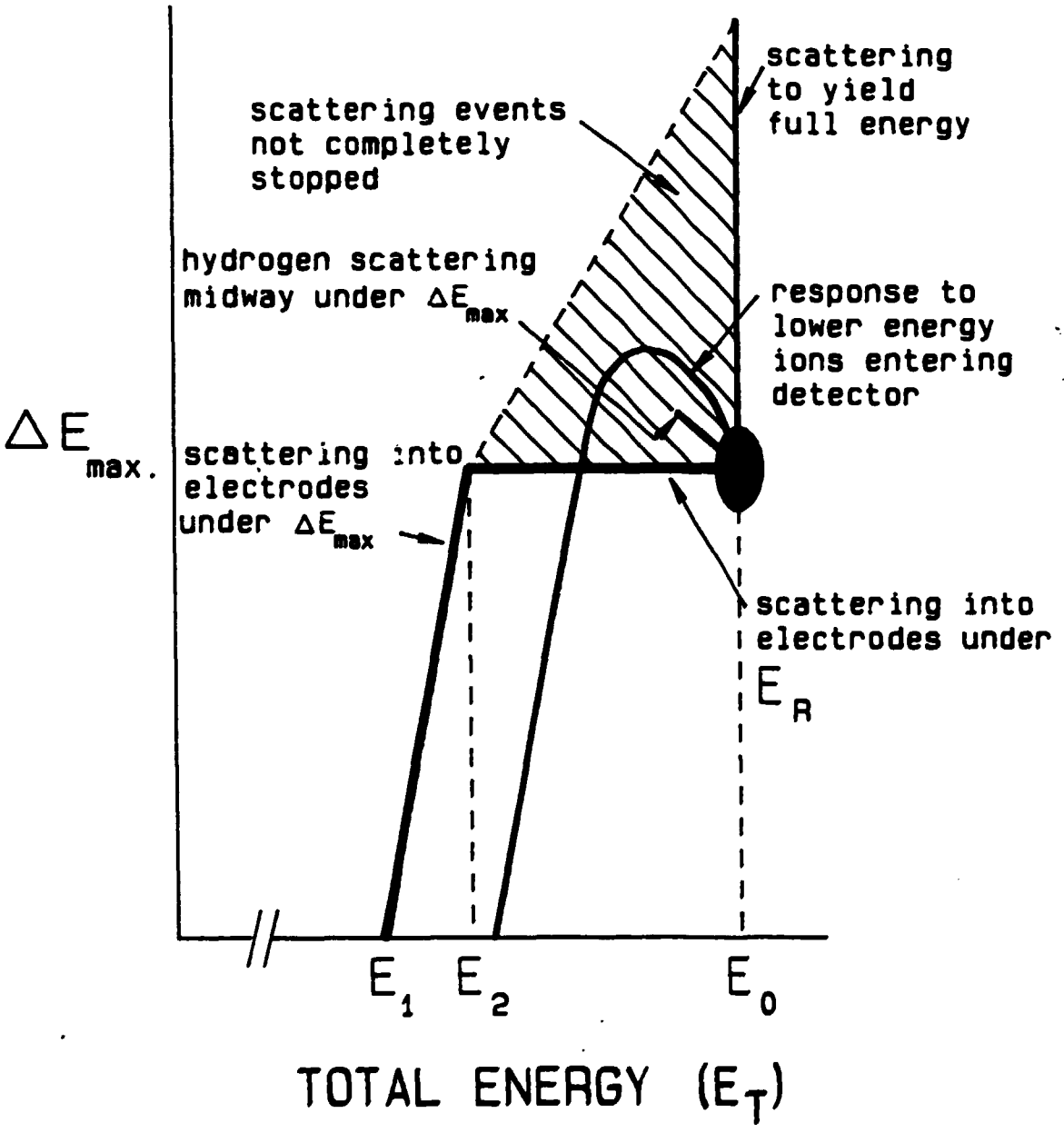
scattering events not completely stopped
hydrogen scattering midway under ΔE max
ΔE max.
scattering into electrodes under ΔE max
scattering to yield full energy
response to lower energy ions entering detector
scattering into electrodes under E R
E 1
E 2
E 0
TOTAL ENERGY (E T)

Fig. 16

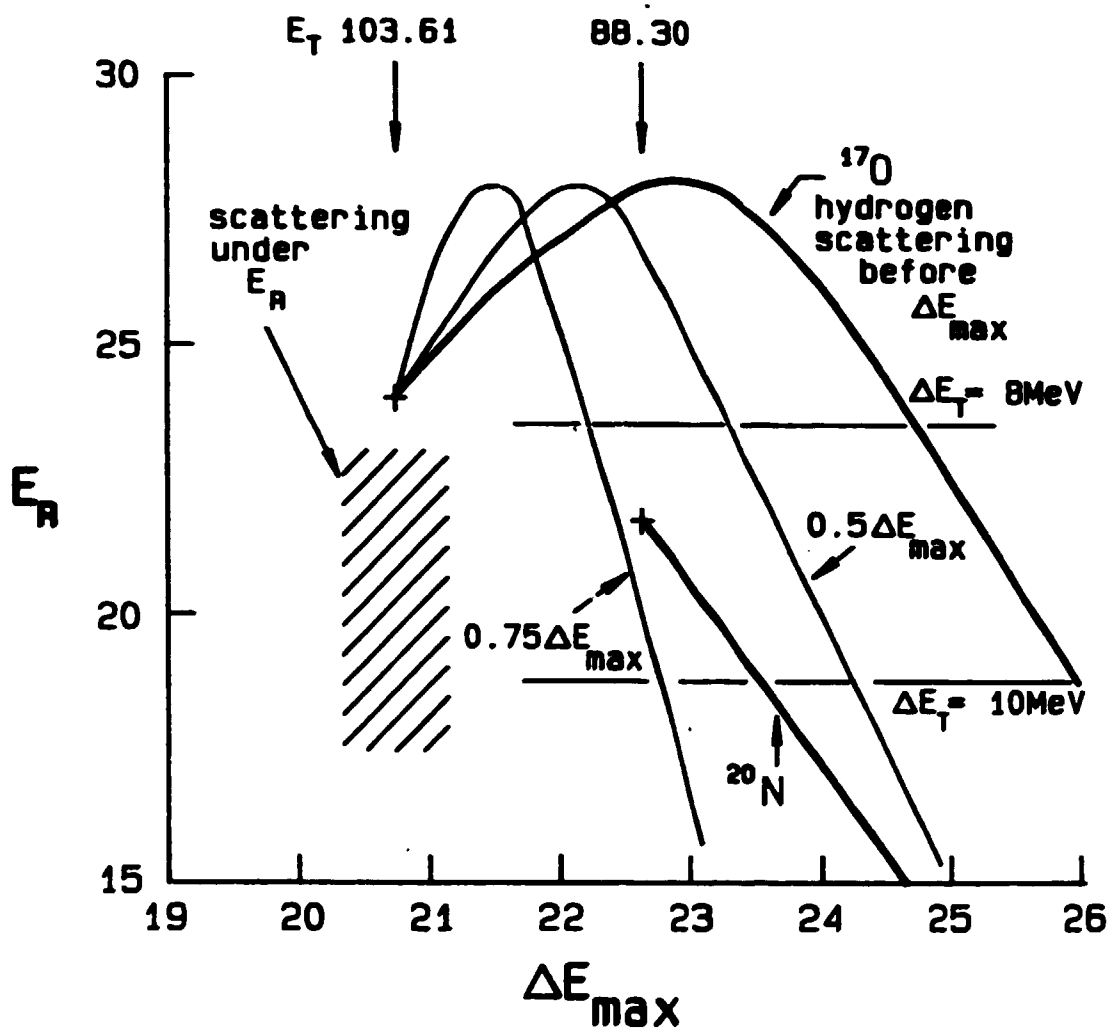
E_T 103.61
88.30
30
25
20
15
E_R
scattering under E_R
^{17}O hydrogen scattering before ΔE_{max}
ΔE_T= 8MeV
$0.5\Delta E_{max}$
$0.75\Delta E_{max}$
ΔE_T= 10MeV
^{20}N
19
20
21
22
23
24
25
26
ΔE_{max}

Fig. 17

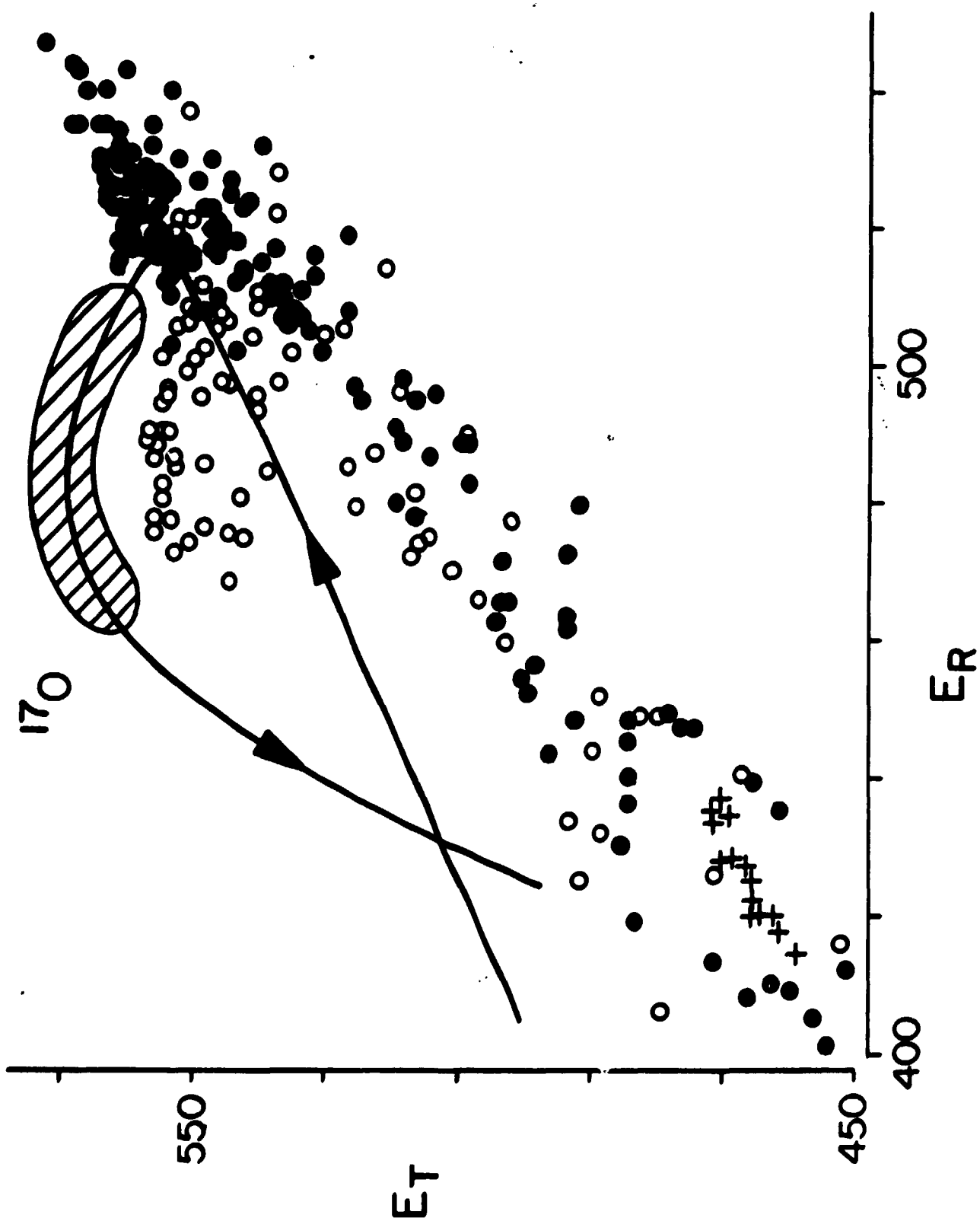
17O
550
450
ET
400
500
ER

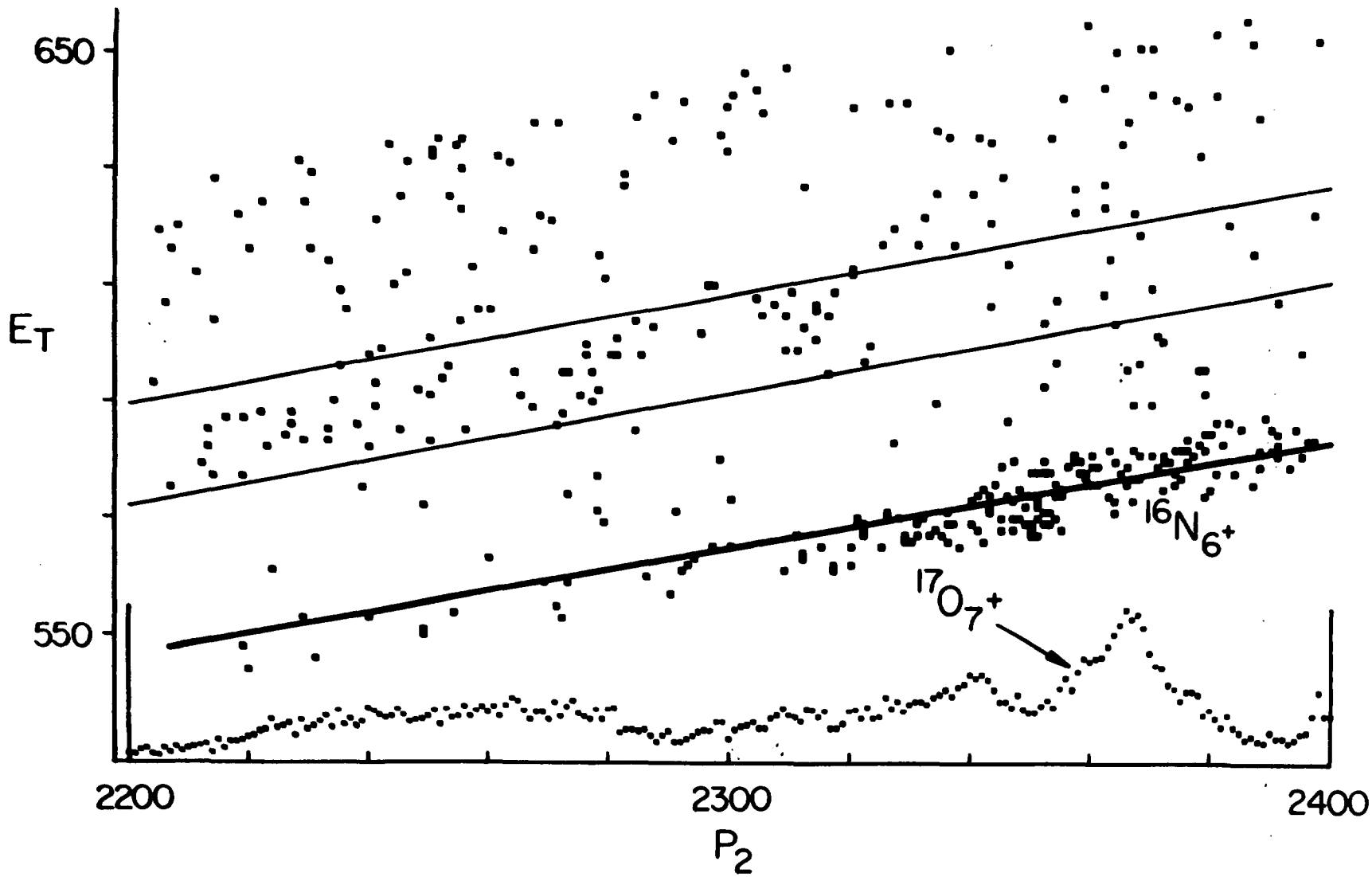

Fig. 19

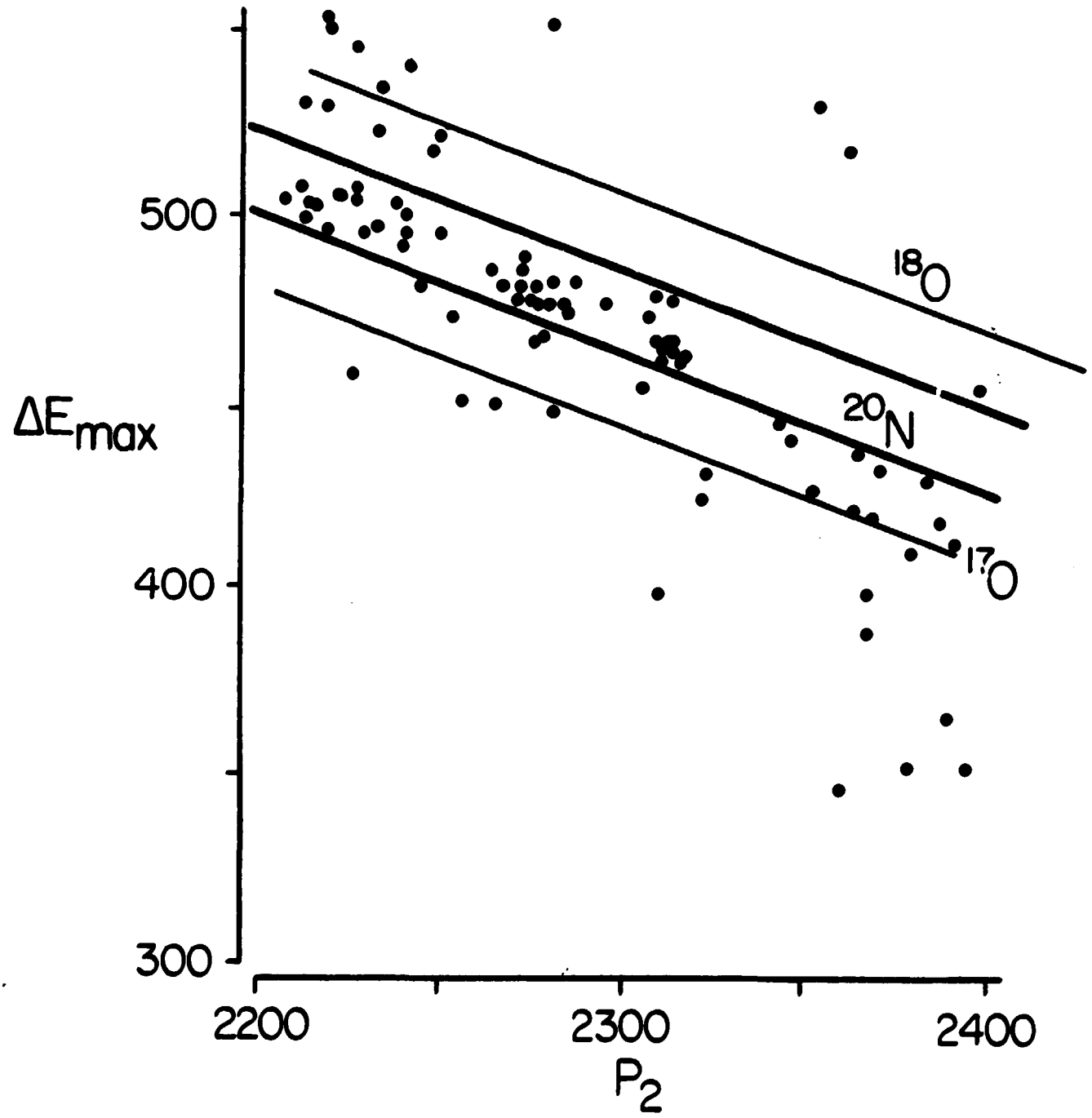

Fig. 20